



Martin Tazreiter, BSc

Proton conductivity measurements on standard and custom ionomers

MASTER'S THESIS

to achieve the university degree of

Master of Science

Master's degree programme: Technical Physics

submitted to

Graz University of Technology

Supervisor

Ass.Prof. Dr. Anna Maria Coclite

Co-supervisor

Ao.Univ.-Prof. Dipl.-Ing. Dr.techn. Roland Resel

Institute for Solid State Physics

AFFIDAVIT

I declare that I have authored this thesis independently, that I have not used other than the declared sources/resources, and that I have explicitly indicated all material which has been quoted either literally or by content from the sources used. The text document uploaded to TUGRAZonline is identical to the present master's thesis.

Date

Signature

1 Acknowledgement

I thank my supervisor Anna Maria Coclite for giving me the opportunity to write this thesis and using techniques of her expertise such as initiated chemical vapor deposition (iCVD), ellipsometry and infrared spectroscopy. She sovereignly supervised me and motivated me whenever it was appropriate. I also acknowledge my co-supervisor Roland Resel for his help regarding X-Ray measurements.

Second, I thank Paul Christian for all the discussions and his superior help regarding all experimental techniques as well as the data evaluation process. Many thanks also goes to Katrin Unger, who helped me especially at the beginning of the thesis with her clear reasoning. I also acknowledge the other members of the CVD-ALD (chemical vapor deposition, atomic layer deposition) group who joined the group during the summer semester break 2016, namely Paul Salzmann, Julian Pilz and Stephan Tumphart for great working atmosphere within the office. Also help from Harald Kerschbaumer, Birgit Kunert, Elisabeth Stern and Robert Schennach is gratefully appreciated.

Last but not least, I thank my parents Marianne and Josef as well as Maria Hirner for their support and motivating words throughout my whole study.

2 Abstract

Membranes of ion conductive materials are essential components in fuel cells and all-solid-state batteries, which are part of a CO₂ neutral energy cycle given that the fuel and electric energy are produced in a renewable manner. The type of ion conductive material investigated in this thesis is called ionomer, which is a polymer containing ions. These ions move if voltage is applied giving rise to electric current. More specifically, the investigated ionomers contain acid groups attached to the polymer structure which are ionized in the presence of water molecules. The ion is therefore H⁺ surrounded by water molecules. This type of ionomer could be applied in a proton exchange membrane fuel cell. The ionomers were deposited by initiated Chemical Vapor Deposition (iCVD), which is a vacuum-based solvent-free technique to produce thin films of homo- or copolymers. The main goal of the thesis was to measure the conductivity of these ionomers. Since the measurement setup was new, preliminary measurements on a well known membrane (*Nafion*TM) were performed. The challenge of measuring the conductivity of the custom ionomers was related to the fact that iCVD films are generally thin (< 2 μm) due to low deposition rates. The low thickness compared to a free standing membrane (> 15 μm) yielded high resistance values and made it difficult to connect to the electrodes. Manual connection of the thin films was avoided by depositing the ionomers directly onto printed circuit boards (PCBs) already containing electrodes. The highest conductivity value achieved was 8 mS/cm for a copolymer deposited by using *methacrylic acid* (MAA), *ethylene glycol dimethacrylate* (EGDMA) as cross-linker and *2-hydroxyethyl methacrylate* (HEMA) as hydrophilic monomer.

3 Kurzfassung

Ionen leitende Membranen sind wichtige Komponenten in Brennstoffzellen und Festkörperakkumulatoren welche Teil eines CO₂ neutralen Kreislaufes sind vorausgesetzt der Brennstoff und die elektrische Energie werden erneuerbar hergestellt. In dieser Arbeit wurden Ionomere untersucht, welche Ionen enthaltende Polymere sind. Wenn eine Spannung anliegt bewegen sich diese Ionen durch das Polymer wodurch elektrischer Strom entsteht. Die untersuchten Ionomere beinhalten Säuregruppen, welche in der Umgebung von Wasser deprotonieren. Das Ion ist deswegen H⁺ umgeben von Wassermolekülen. Dieser Ionomer-Typ könnte in Protonenaustauschmembran-Brennstoffzellen verwendet werden. Die Ionomere wurden anhand initiiertes chemischer Gasphasenabscheidung (iCVD, initiated chemical vapor deposition) synthetisiert. Dieses vakuum-basierte und lösungsmittelfreie Verfahren erlaubt die Herstellung dünner Schichten aus Homo- und Copolymeren. Das Hauptziel dieser Arbeit war die Messung der Leitfähigkeit dieser Schichten. Da der Messaufbau neu war wurden zuerst Messungen an einer gut bekannten Probe (*Nafion*TM) durchgeführt. Die Schwierigkeit bei der Messung der Leitfähigkeit der eigenen Ionomere bestand darin, dass die Schichten wegen der geringen Depositionsrate sehr dünn sind (< 2 µm). Die verglichen mit frei stehenden Membranen (> 15 µm) geringe Dicke führt zu hohem Widerstand und erschwert die Verbindungsherstellung zu den Elektroden. Eine manuelle Kontaktierung wurde durch direktes Aufbringen des Ionomers auf Leiterplatten mit Elektroden verhindert. Die höchste erreichte Leitfähigkeit beträgt 8 mS/cm und wurde an einem Copolymer gemessen, welches mit *methacrylic acid* (MAA), *ethylene glycol dimethacrylate* (EGDMA) als vernetzendes Monomer und *2-hydroxyethyl methacrylate* (HEMA) als hydrophiles Monomer hergestellt wurde.

Contents

1	Acknowledgement	3
2	Abstract	4
3	Kurzfassung	5
4	Motivation	8
5	Theory	9
5.1	Theory of Impedance Spectroscopy	9
5.1.1	Conductivity	9
5.1.2	Two point versus four point measurements	10
5.1.3	Equivalent circuit of AC two point measurements	12
5.1.4	Parallel current paths	14
5.2	Theory of Polymers	15
5.3	Theory of proton conduction in ionomers	16
5.4	Theory of initiated chemical vapor deposition	17
6	Experimental details	18
6.1	Impedance spectroscopy setup	18
6.2	Fourier transform infrared spectroscopy	22
6.3	Ellipsometry	26
6.4	Initiated chemical vapour deposition	27
6.5	Chemicals	28
6.6	Substrates and deposition conditions	29
7	Preliminary measurements	34
7.1	Mesurements of water	34
7.2	Measurements on <i>Nafion</i>	36
8	Results	39
8.1	Swelling behavior investigated by spectroscopic ellipsometry	39
8.2	Impedance spectroscopy results of series 1 and 2	40
8.3	Impedance spectroscopy results of series 3, p-MAA-EGDMA	41
8.4	Thickness and volume fraction variations in iCVD reactor of p-MAA-EGDMA, deposition 28 of series 3	43

8.5	Impedance spectroscopy results of series 4, p-MAA-EGDMA-HEMA	44
8.6	Results of morphologic investigations	46
8.7	Results of X-Ray experiments	49
9	Conclusions	50
	References	50
10	Appendix	52
10.1	Desposition conditions of series 1 and 2	52
10.2	List of coding software	53
10.3	Python scripts for FTIR measurements	53
10.4	R script for FTIR baselinecorrection	57

4 Motivation

Proton conductors contain mobile cations, which move if an electric field is applied. There are liquid as well as solid proton conductors and for applications, the latter is often preferred due to enhanced stability. Special types of ceramics, polymers and since recently also polymerized ionic liquids [1] are known to provide these cations. In the case of polymers, acid groups incorporated in the polymer structure can be ionized if the polymer absorbs water. These ions are then available as charge carriers as depicted in figure 1. Ionomers can be used as membranes in supercapacitors [2] as well as proton exchange membrane fuel cells (PEMFCs) as depicted in figure 2, which transform chemical energy to electrical energy or vice versa.

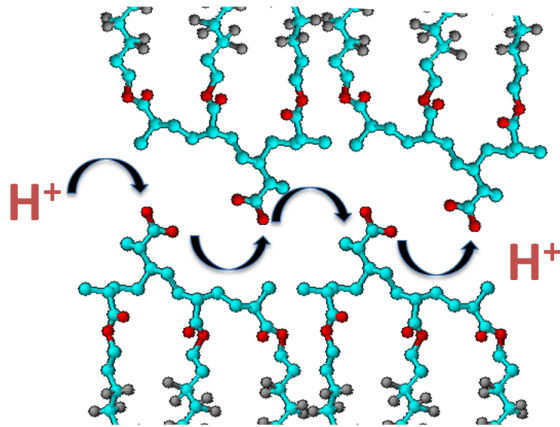


Figure 1: Acid groups ionized by water provide charge carriers and therefore proton conductivity, reprinted from [3]

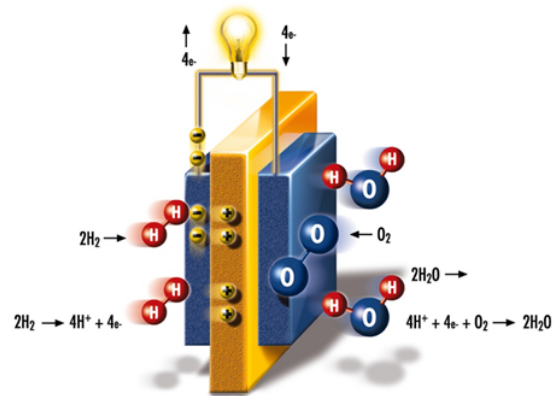


Figure 2: Working principle of a proton exchange membrane fuel cell¹

The membrane separates two electrically conducting electrodes at different electric potentials. Therefore, the membrane shall not conduct electrons, otherwise the electrodes would be short-circuited. On the other hand, high proton conductivity is important to reduce the ohmic loss in the membrane to maximize the output voltage of the fuel cell. This application, among others, motivates to create a material with high proton conductivity as well as chemical and mechanical stability.

In the group of *Ass.Prof.Dr. Anna Maria Coclite, Institute for Solid State Physics at Graz University of Technology*, thin layers of polymers get deposited by *initiated*

¹<http://www.h-tec.com/en/education/technology/fuel-cells/>

chemical vapor deposition (iCVD). If acid groups are incorporated, ion conductivity can be achieved with this technique as shown in references [3] and [4]. The aim of this thesis was to optimize the setup for the measurement of proton conductivity, to achieve a fast and reliable materials development process.

5 Theory

5.1 Theory of Impedance Spectroscopy

5.1.1 Conductivity

Conductivity is a microscopic local material property denoted by σ . It is used for the microscopic Ohms law stated as

$$\vec{j} = \sigma \vec{E} \quad (1)$$

In general, it is a rank two tensor depending on position, but for simplicity, lets assume an isotropic medium with a constant conductivity inside its boundary and zero on the outside. If in addition the geometry of the medium is as simple as shown in figure 3 and the electric field is a constant vector pointing along l inside the medium, the total current through the area $A = ab$ is given by

$$I = |\vec{j}|A \quad (2)$$

and the conductivity is given by

$$\sigma = \frac{1}{\rho} = \frac{l}{AR} = ne\mu \quad (3)$$

Table 1: Definition of variables

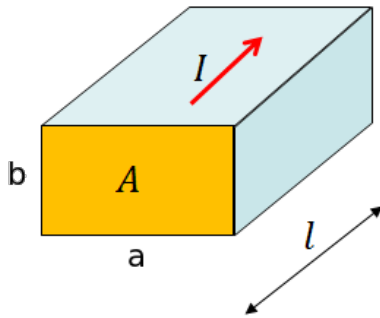


Figure 3: Cuboidal geometry with homogeneous current density

name	symbol	unit
current density	\vec{j}	Am^{-2}
electric field	\vec{E}	Vm^{-1}
conductivity	σ	$\Omega^{-1}\text{m}^{-1}$
resistivity	ρ	Ωm
width	a	m
thickness	b	m
length	l	m
area	A	m^2
resistance	R	Ω
charge carrier density	n	Asm^{-3}
elementary charge	e	As
mobility	μ	$\text{m}^2\text{V}^{-1}\text{s}^{-1}$

5.1.2 Two point versus four point measurements

The most simple resistance measurement setup is a two point direct current (DC) measurement setup as shown in figure 4. The gray block represents the object of which the resistance should be measured. If this object is a usual electron-conductive ohmic resistor, the contact impedances Z_c , as depicted in figure 5, can be often modeled as ohmic resistors. If this contact resistance is much less than the objects resistance, the latter can be approximated by dividing the applied voltage through the measured current.

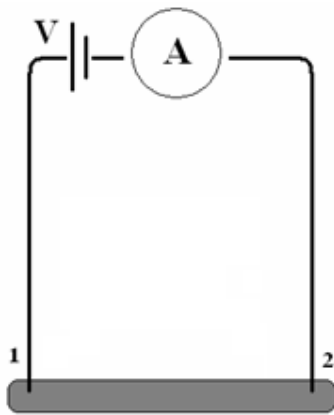


Figure 4: Two point measurement setup
 V .. voltage source
 A .. ampere-meter

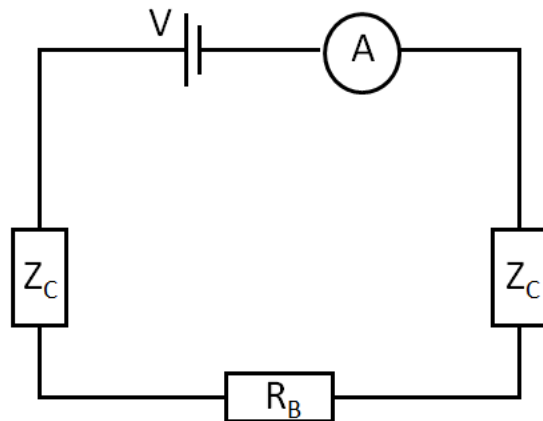


Figure 5: Two point equivalent circuit
 Z_C .. contact impedance
 R_B .. bulk resistance

If the object is an electrolyte instead, the circumstances are more complicated. The current is carried by electrons in the wires and by ions in the electrolyte. If current passes through the interface between electrodes and electrolyte, electrochemical reactions occurring at the interfaces act as sources and sinks for the electrons and ions. In this case, the contact impedances have non-linear current voltage characteristics, which is often described by the Butler Volmer Equation [5]. Therefore the two-point DC measurement is not suitable to determine the bulk resistance. However a two-point alternating current (AC) measurement can be performed at small voltages to avoid non-linear behavior and at different frequencies to be able to distinguish the contact impedance from the bulk impedance. This measurement is called two-point impedance spectroscopy.

A different method to determine the bulk resistance is a four-point measurement as shown in figure 6 with its equivalent circuit shown in figure 7, since the influence of the interfaces can almost be eliminated by using it. Compared to the two-point setup, there is an additional voltmeter, which measures the voltage between point 2 and 3 and has in the ideal case infinite input impedance. In this case, there is no current flowing through the contact impedances connecting the voltmeter to the ion-conductor in figure 7 and the measured voltage is exactly the voltage drop across the inner bulk resistor. In the same approximation of infinite input impedance of the voltmeter, the measured current is exactly the current through the inner bulk resistor. This leads to a linear behavior of the current versus the measured voltage, of which the bulk resistance follows directly

using Ohm's law. This method works for both DC and AC. The AC impedance spectroscopy still has the advantage of using small voltages and therefore avoiding electrochemical reactions.

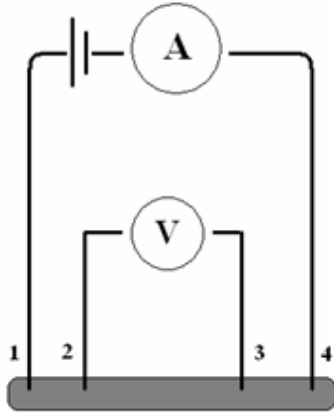


Figure 6: Four-point measurement setup
A .. ampere-meter
V .. voltmeter

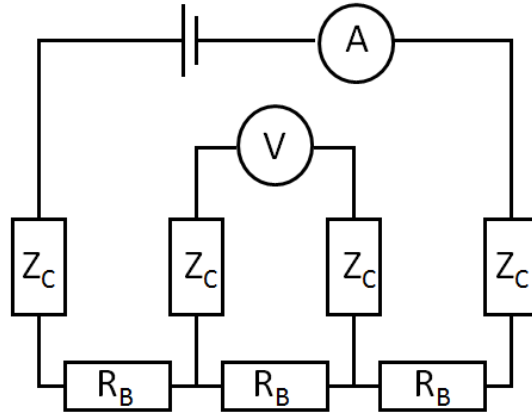


Figure 7: Four-point equivalent circuit
 Z_C .. contact impedance
 R_B .. bulk resistance

5.1.3 Equivalent circuit of AC two point measurements

If an AC two point measurement of an electrolyte is performed, or more precisely of an ionomer, the data should be fitted with the frequency dependent impedance of the equivalent circuit as shown in figure 5 but taking into account the capacity between the electrodes, which is not seen in a DC measurement. The contact impedance can be specified using the standard circuit elements as shown in table 2 and the impedance of the whole circuit can be calculated by iteratively applying the circuit rules giving the impedance Z of a circuit consisting of two impedances Z_1 and Z_2 :

- Parallel circuit:

$$Z = Z_1 \parallel Z_2 = \frac{1}{\frac{1}{Z_1} + \frac{1}{Z_2}} \quad (4)$$

- Serial circuit:

$$Z = Z_1 + Z_2 \quad (5)$$

Table 2: Circuit elements

R .. resistance

C .. capacitance

L .. inductance

P .. phasance

ω .. angular frequency

name	impedance	phase φ / radians	symbol
resistor	R	0	
capacitor	$\frac{1}{i\omega C}$	$-\frac{\pi}{2}$	
inductor	$i\omega L$	$\frac{\pi}{2}$	
constant phase element	$(i\omega)^{\frac{2}{\pi}\varphi} P$	φ	

The *constant phase element* (CPE) is a generalization of the first three [6], which have special values of φ . This constant phase element can be used to model the contact impedance which leads to a two point equivalent circuit as shown in figure 8.

The upper part shows a capacitor, which symbolizes the capacity of two electrodes surrounded in the electrolyte with a specific relative dielectric constant (sometimes called *geometrical capacitance*). The process of ions moving through the electrolyte and accumulating at the interfaces to the electrodes is happening in parallel. Each interface is modeled with the same CPE assuming mirror symmetry and

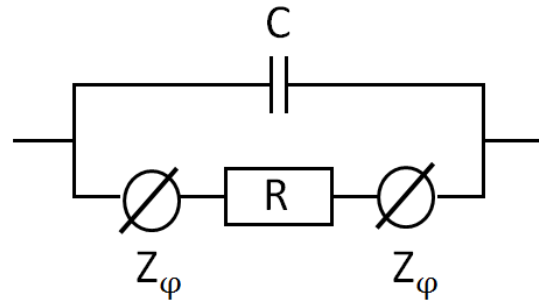


Figure 8: Two point equivalent circuit for electrolyte measurements

the drift of ions is modeled with an ohmic resistor. In the ideal case, the contact impedance is just a capacitor, but since this capacitor is not ideal, it is better to use the CPE. Using parallel and serial circuit rules and table 2, the impedance of

this circuit is calculated as shown in equation 6.

$$Z = \frac{1}{\frac{1}{R + 2(i\omega)^{\frac{2}{\pi}} \varphi P} + i\omega C} \quad (6)$$

The model is very similar to the circuit shown in figure 1.3.1(d) of [7], dropping the charge transfer resistance parallel to the interface and using the more general constant phase element as interface impedance instead of a pure capacitor. If electrochemical reactions would occur at the interfaces, the charge transfer resistance (or reaction resistance) parallel to the CPE would be necessary.

5.1.4 Parallel current paths

Since the ionomers studied in this work all need to absorb water in order to conduct ions, they have to be measured in a medium such as liquid water or humidified gas. The current flowing through the measurement cell can split in two parts, the first one going through the membrane as desired, the second one going through the medium. The actually measured resistance is

$$R_{\text{total}} = R_{\text{ionomer}} \parallel R_{\text{medium}} \quad (7)$$

The resistance of the medium R_{medium} has to be measured after the measurement of the ionomer, since impurities could have lowered the medium resistance when the first measurement was performed. The ionomer resistance R_{ionomer} can then be calculated by

$$R_{\text{ionomer}} = \frac{1}{\frac{1}{R_{\text{total}}} - \frac{1}{R_{\text{medium}}}} \quad (8)$$

If $R_{\text{total}} \ll R_{\text{medium}}$ the influence of these parallel currents can be neglected, which means $R_{\text{ionomer}} \approx R_{\text{total}}$.

5.2 Theory of Polymers

Polymers are materials consisting of chains of one or more repeating units covalently bonded together. The repeating units are called **monomers** and the process of binding them together is called **polymerization**. There are synthetic polymers used in everyday life and natural polymers essential to all known forms of life itself. The most common and also most simple synthetic polymer is polyethylene which is used for example in packaging. Its chemical structure is shown in figure 9. The repeating unit shows the polymerized version of the monomer ethene. A bit more complicated is the chemical structure of polystyrene as shown in 10.

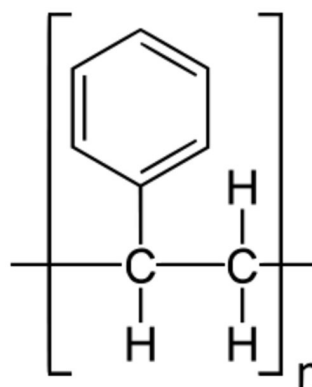
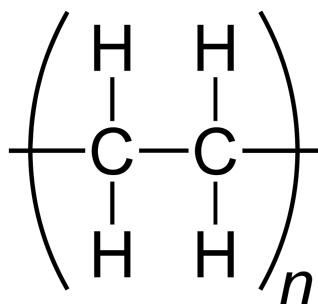


Figure 9: Chemical structure of polyethylene² Figure 10: Chemical structure of polystyrene³

An examples for a natural polymer is cellulose which is a structural component in plants, see figure 11. Another example is deoxyribonucleic acid (DNA), a basic building block of all known forms of live. Its schematically drawn in figure 12.

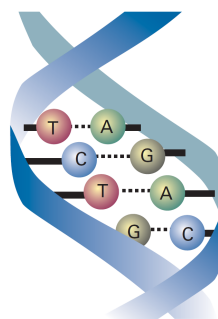
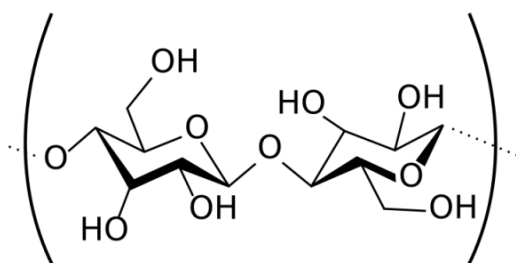


Figure 11: Chemical structure of cellulose⁴ Figure 12: Sketch of DNA reprinted from [8]

¹https://commons.wikimedia.org/wiki/File:Polyethylene_repeat_unit.svg

³http://www.icf.biz/EPS_XPS_NEOPOR.html

If a polymer consists of only one monomer species it is called homopolymer. If it consists of more than one monomer, it is called copolymer. Copolymers consisting of two monomer species A and B can be classified according to their order in which the repeat units are joined together.

- Alternating copolymers: ..-A-B-A-B-..
- Statistic copolymers: The sequence is generated randomly like ..-A-A-B-B-B-A-B-A-A-B-..
- Block copolymer: One homopolymer chain of each kind covalently bond together ..-A-A-A-B-B-B-..
- Graft copolymer: Side chains of one species bond to the main chain of the other species

5.3 Theory of proton conduction in ionomers

The transport of protons in ionomers can be described by three mechanisms, see figure 13

- **Proton hopping or Grotthuss mechanism:** A proton together with a water molecule forms H_3O^+ . If one of the protons jumps to another water molecule due to the presence of an electric field, this water molecule becomes H_3O^+ .
- **Vehicle mechanism:** A proton together with water molecules forms a complex and drifts through the medium.
- **Polymer chain segmental motion:** If the mobile ends of polymer chains carry a negative charge due to for example an ionized acid group, they can collectively carry a proton in the direction of the electric field by moving within their limited range.

⁴<http://chemistry.about.com/od/factsstructures/ig/Chemical-Structures---C/Cellulose.htm>

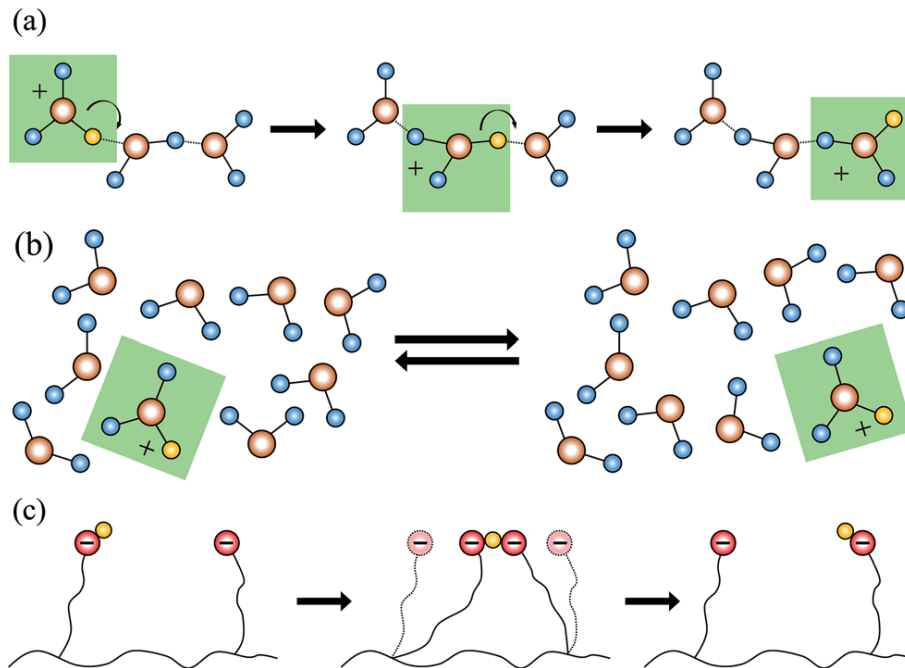


Figure 13: proton transport mechanisms reprinted from [2]

a .. Grotthuss mechanism

b .. Vehicle mechanism

c .. Polymer chain segmental motion

Since the conductivity is directly proportional to the charge carrier density (see equation 3), the latter should be as high as possible. The charge carrier density is given by the density of available ionized acid groups and the availability depends on the distribution of acid groups within the ionomer. If they form channels from one side of the ionomer to the other, the protons can be conducted through.

5.4 Theory of initiated chemical vapor deposition

Initiated chemical vapor deposition (iCVD) is a versatile method to produce thin polymer coatings [9]. It is a vacuum-based **free radical polymerization** process, which means that the polymerization is initiated by radicals within a vacuum chamber. The radicals can be produced by thermally splitting initiator molecules at a heated filament. Monomers have to be supplied during the whole deposition. Since two simultaneously growing polymer chains can terminate themselves, also initiator molecules have to be supplied during the whole polymerization process. This is done by evaporating both monomers and initiator from the liquid phase and feeding them through lines into the vacuum chamber. Both

monomers and radicals adsorb at the surface of the substrate and start the polymerization process. This process is schematically drawn in figure 14. iCVD is a solvent-free polymerization process. The absence of any solvent allows to coat substrates which would be dissolved by a solvent in case of a solution-based technique. Additionally it avoids possible problems due to different solubilities of the monomers in a solvent. The coatings are very conformal due to surface diffusion of the absorbed species prior to polymerization as well as the lack of any solvent which would cause thickness variations due to surface tension effects.

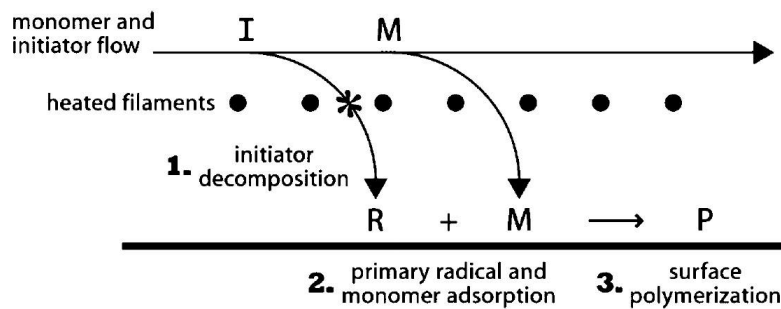


Figure 14: Schematics of iCVD process reprinted from [9]

6 Experimental details

6.1 Impedance spectroscopy setup

The measurement device for impedance spectroscopy (Gamry Instruments, Reference 600) is shown in figure 15 and its working principle in figure 16. The user defines some signal, which is a voltage over time, and is generated in the device. This signal goes to the control amplifier, which controls its output such that the feedback voltage at its negative input equals the signal. The feedback voltage, which is the voltage between the *Reference* and the *Working Sense* electrode, is measured. This seems redundant but this information can be used to check whether the control amplifier works correctly. The current is measured at the shunt resistor R_m .



Figure 15: Gamry potentiostat⁵

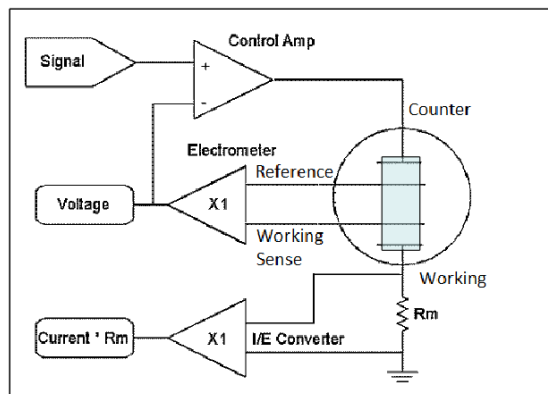


Figure 16: Working principle of the Gamry potentiostat modified from⁶

To measure the in-plane conductivity of Nafion, a conductivity clamp (Scribner Associates, Inc., BT-110) was used as shown in figure 17. It comprises two *Teflon* parts, a main one and a cover. The main part is connected to four platinum wires as shown in figure 18. The inner electrodes have a (more or less) well-defined geometry and the outer ones have platinum grids attached to make even better contact. This is possible since the exact geometry at the outer electrodes is not that important.

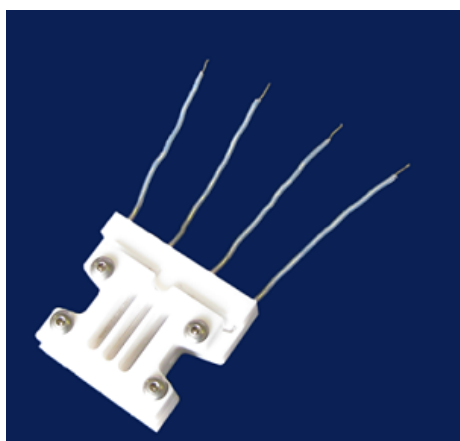


Figure 17: Clamp BT110

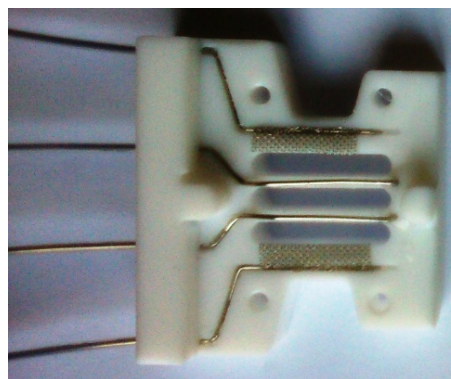


Figure 18: Open conductivity clamp

This clamp was also thought to be used for measuring custom ionomers deposited on flexible substrates, but this technique was too rough for the thin layers of

⁵<http://www.gamry.com/application-notes/instrumentation/potentiostat-fundamentals/>

⁶<https://www.gamry.com/assets/Support-Downloads/Product-Manuals/Reference-600-Operators-Manual.pdf>

~1 μm thickness. For this reason, printed circuit boards (PCBs) were ordered from *Eurocircuits* with a custom layout as shown in figure 19. These PCBs have an *electroless nickel immersion gold* (ENIG) coating to protect them from corrosion. The core material is copper of about 44 μm thickness, covered by approximately 6 μm Ni, covered by about 0.1 μm Au as shown in figure 20. The outer electrodes are the current driving electrodes and the inner four electrodes are voltage sensing electrodes. This design was chosen to allow multi-distance measurements to check the linear relationship of resistance versus distance as done in [10]. These PCBs have the advantage that the custom ionomers can be directly deposited on them and the connection to the electrodes does not happen manually.

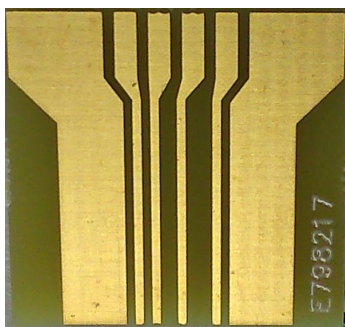


Figure 19: PCB as delivered from Eurocircuits

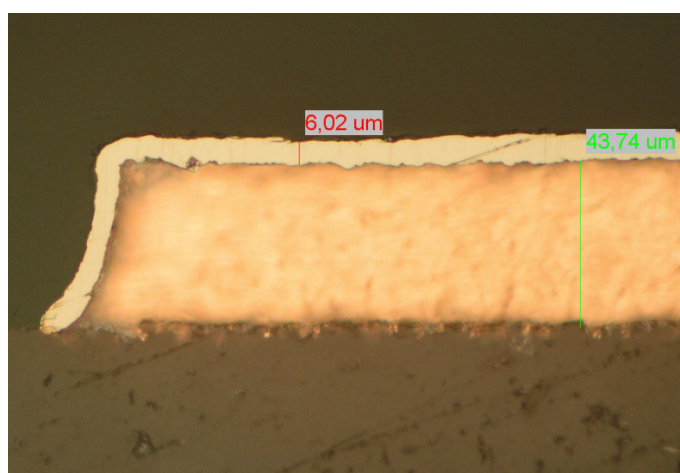


Figure 20: Crossection of PCB⁷

For through-plane measurements, the device shown in figure 21 was used, as described in reference [11]. After locating the ionomer membrane between the electrodes, the cross-section looks like drawn in figure 22. The green part is an isolating material. In this configuration, there are no parallel current paths through the medium. This fact allowed to use a 0.1 molar HCl solution as medium to swell the ionomer, making a stable contact between Pt electrodes and membrane eliminating possible bad connection issues for example due to a not perfectly flat Pt surface.

⁷<http://www.eurocircuits.com/blog/177-How-do-we-assure-the-quality-of-your-PCB---part-3>

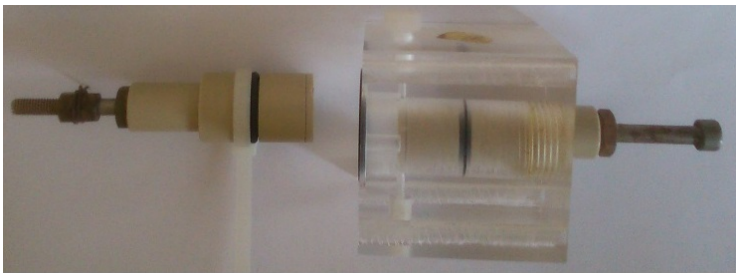


Figure 21: Throughplane measurement device

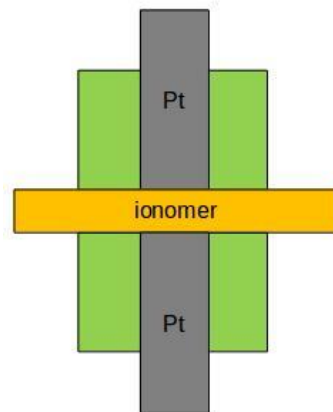


Figure 22: Throughplane measurement device crosssection

As a measurement cell for inplane measurements, a glass jar with metal enclosure was used. This cell can be used in two different modes: the liquid water mode (figure 23) and the humidity mode (figure 24). In the humidity mode, either deionized water or a saturated KCl solution was used. Figure 25 shows the humidity as a function of time in both cases. This data was measured with the SHT15 sensor at a temperature of $T = (24.5 \pm 0.5) \text{ }^\circ\text{C}$. In the case of deionized water, the relative humidity converges to $\text{RH} = 100 \%$ as it is defined, whereas in the case of saturated KCl solution, it converges to $\text{RH} = (88 \pm 2) \%$. This value is slightly off the literature value of $\text{RH} = (84.34 \pm 0.26) \%$ ⁸.

⁸<http://www.omega.com/temperature/z/pdf/z103.pdf>

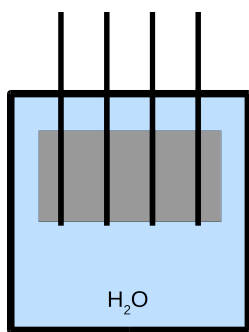


Figure 23: Measurement cell using water

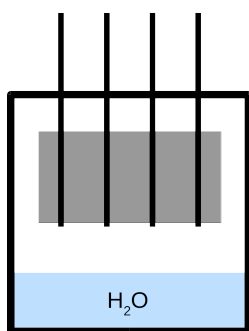


Figure 24: Measurement cell using humid air

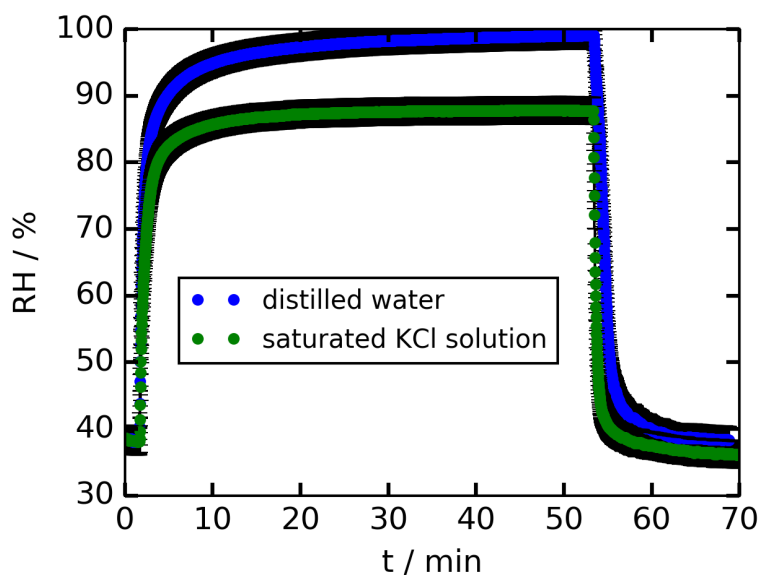


Figure 25: Relative humidity as a function of time in measurement cell

6.2 Fourier transform infrared spectroscopy

Fourier transform infrared spectroscopy (FTIR) was used to determine the volume fraction of the custom ionomers. The technique is based on the measurement of the absorption of infrared light transmitted through the ionomer and the Si substrate at different wave-numbers $\tilde{\nu}$ in the range of 700-4000 cm^{-1} (limited by the FTIR spectrometer, Bruker IFS 66 v/s). This range corresponds to an energy range of about 87 to 496 meV by the equation

$$E = hc\tilde{\nu} \quad (9)$$

Chemical bonds have characteristic vibrational modes with energies in this range and are therefore excited. They also re-emit infrared light, but into a random direction, therefore intensity is missing at the detector at well defined wavenumbers, which is measured as absorption spectrum. An exemplary spectra of the full measurable wavenumber range with labeled peaks is shown in figure 26 (this spectrum is baseline corrected as discussed later). The assignment of the

peaks was performed according to [12]. The intensities of the O-H peaks were fluctuating from measurement to measurement maybe due to some frozen water in the liquid N₂ cooled detector. The monomer specific peaks are located between 1000 and 2000 cm⁻¹. More specifically, methacrylic acid (MAA) and ethylene glycol dimethacrylate (EGDMA) can be distinguished by the peaks at 1730 and 1703 cm⁻¹ which overlap considerably, whereas 2-hydroxyethyl methacrylate (HEMA) has a peak at 1075 cm⁻¹.

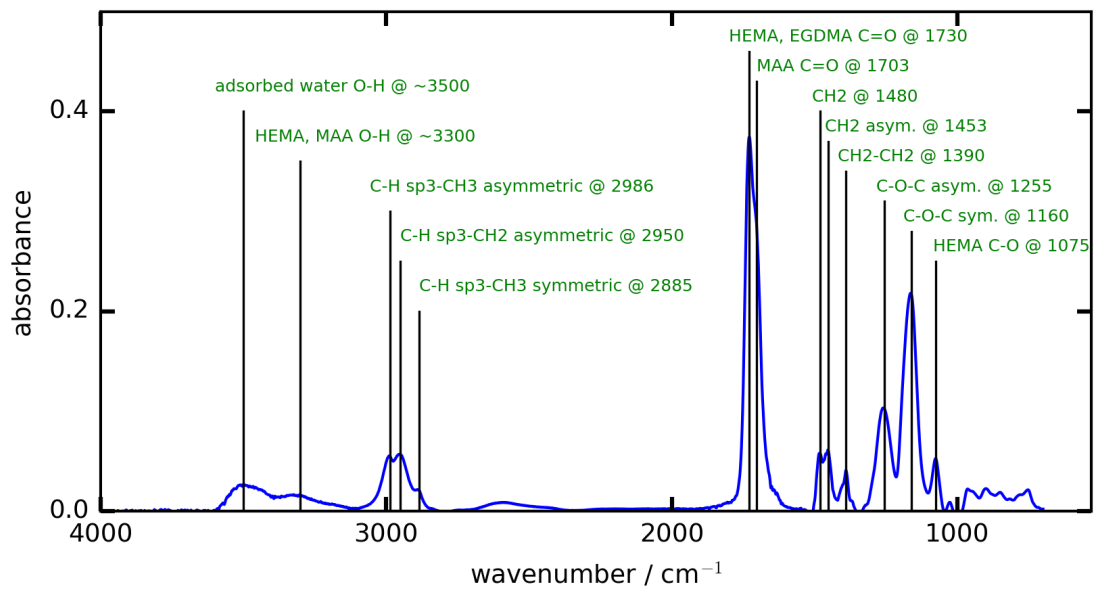


Figure 26: FTIR absorption spectrum of exemplary p-MAA-EGDMA-HEMA (dep32.2) with labeled peaks

To be able to extract the volume fraction of the individual monomers within the copolymer, some theory has to be considered. A wavenumber dependent *Beer-Lambert* law describing the intensity decrease caused by $N + 1$ species with absorption coefficient A_i states:

$$I(\tilde{\nu}) = I_0(\tilde{\nu})e^{-\sum_{i=1}^{N+1} A_i(\tilde{\nu})d_i} \quad (10)$$

where $I_0(\tilde{\nu})$ is the intensity of the incoming light and $I(\tilde{\nu})$ is the intensity of the outgoing light which is measured indirectly by the FTIR technique. The $(N + 1)^{\text{th}}$ species is the Si substrate. Each species is the polymerized version of a monomer and full polymerization is assumed. It is helpful to first also assume that all $N+1$ species are separated into layers of thickness d_i , but as evident from equation 10, the measured $I(\tilde{\nu})$ would not change if the layers are

intermixed to an arbitrary concentration dependence in transmission direction, using the assumption that the total polymer volume does not change during the mixing process. The influence of the Si substrate can be eliminated by a reference measurement measuring only Si:

$$I_{Si}(\tilde{\nu}) = I_0(\tilde{\nu})e^{-A_{N+1}(\tilde{\nu})d_{N+1}} \quad (11)$$

By dividing equation 10 by 11 one eliminates the Si influence as well as $I_0(\tilde{\nu})$ which depends on the infrared source:

$$\frac{I}{I_{Si}} = e^{-\sum_{i=1}^N A_i(\tilde{\nu})d_i} \quad (12)$$

Taking the logarithm, multiplying by -1 and calling it ionomer absorption spectrum $A(\tilde{\nu})$ one gets

$$A(\tilde{\nu}) = \sum_{i=1}^N A_i(\tilde{\nu})d_i = -\ln\left(\frac{I}{I_{Si}}\right) \quad (13)$$

which can be calculated from the two measurement data sets. Up to now, the equations describe the most general case of a copolymer consisting of N species. By depositing each species separately, measuring its absorption spectrum and dividing by the layer thickness (measured with ellipsometry), the absorption spectrum per unit length A_i of the individual species was determined. Using the A_i as basis functions to fit the absorption spectra of a copolymer by linear least square method, the (hypothetical) individual thicknesses d_i are determined. The total thickness of the copolymer is given by

$$d = \sum_{i=1}^N d_i \quad (14)$$

and the volume fraction of species i is given by

$$F_i = \frac{d_i}{d} \quad (15)$$

The volume fraction calculation was implemented in Python, see section 10.3, which requires an R script baseline-correcting the absorbance spectra, see section 10.4. The baseline-correction was done by subtracting the baseline to eliminate interference effects, for example the copolymer can act as anti-reflecting coating with negative absorbance as shown in figure 27. All shown ionomer absorption spectra shown in this thesis are baseline-corrected in that manner.

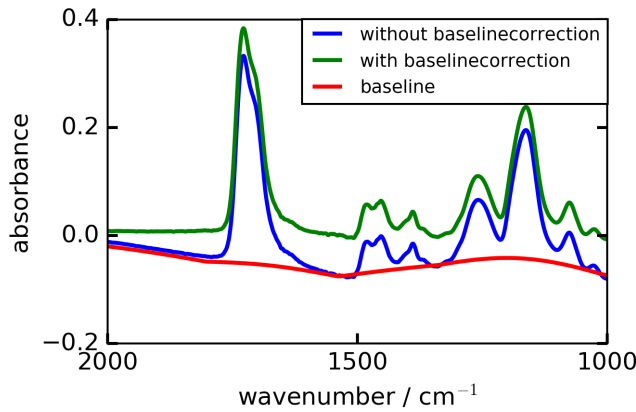


Figure 27: Exemplary ionomer absorption spectrum with baseline correction

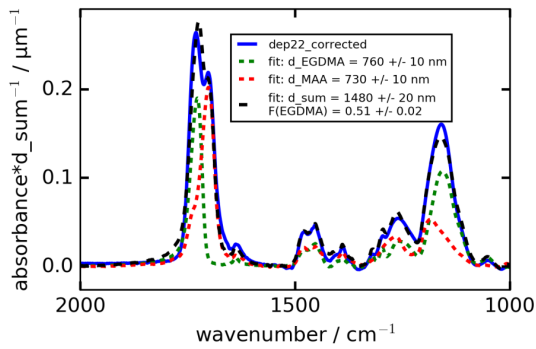


Figure 28: Ionomer absorption spectrum of p-MAA-EGDMA (FTIR)

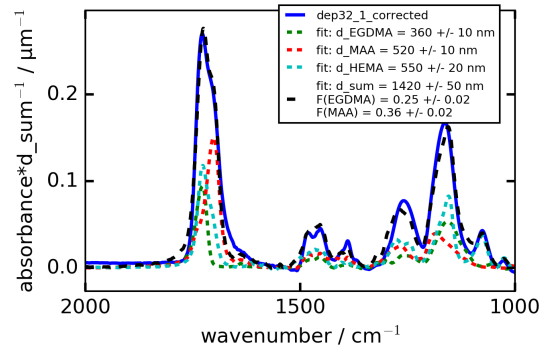


Figure 29: Ionomer absorption spectrum of p-MAA-EGDMA-HEMA (FTIR)

An example of a linear least square fit to yield volume fractions with two monomers is shown in figure 28. One with three monomers in figure 29. The total thickness d measured with FTIR was compared to the thicknesses of the same samples measured with ellipsometry, which is the most accurate thickness measurement technique performed, see figure 30. The relative deviation RD of the FTIR thicknesses d_{FTIR} from the ellipsometry thicknesses $d_{\text{Ellipsometry}}$ as calculated by equation 16 is plotted in figure 31. The standard deviation is less than 10 %, which is satisfactory since the thicknesses depend on the relative humidity, which was not controlled during the ellipsometry measurements.

$$\text{RD} = \frac{d_{\text{FTIR}} - d_{\text{Ellipsometry}}}{d_{\text{Ellipsometry}}} \quad (16)$$

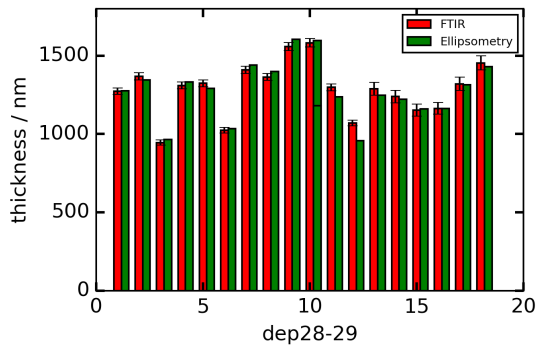


Figure 30: Comparison of thicknesses measured with FTIR versus Ellipsometry

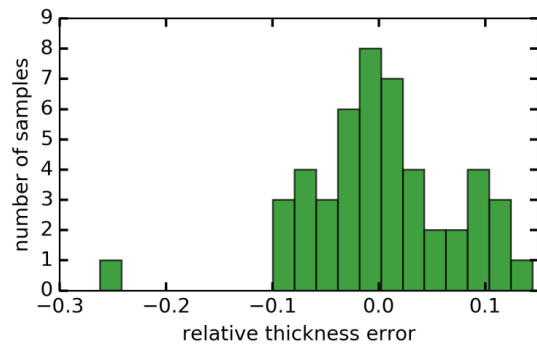


Figure 31: Histogram of relative deviation of thicknesses measured with FTIR compared to Ellipsometry

6.3 Ellipsometry

Ellipsometry was performed on the custom ionomers with Si substrates primarily to determine the thickness of the ionomers, but it also gives roughness and index of refraction. The basic setup is depicted in figure 32.

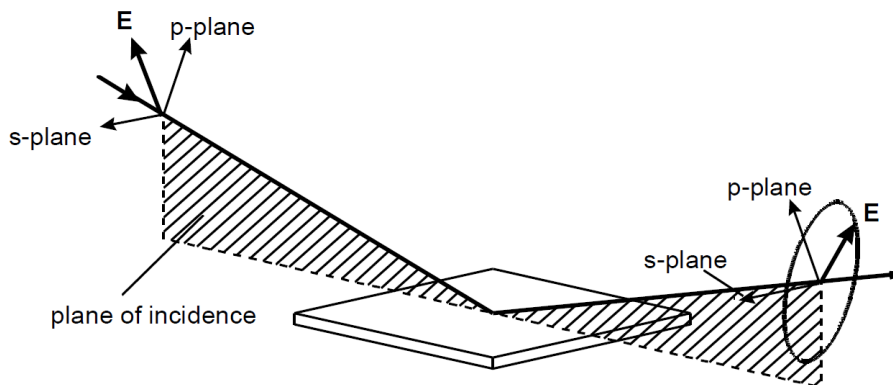


Figure 32: Ellipsometry setup redrawn from ⁹

Broad band linear polarized light (wavelength range of 371-1000 nm given by ellipsometry device, M-2000V, J.A. Woollam Co.Inc.) is headed onto the sample and the spectrum of the reflected light is measured during a full turn of the analyzing polarization filter. At each wavelength, the square root of the intensity (which is proportional to the electric field) as a function of analyzing angle describes an ellipse which is parameterized using equation 17, where Ψ and Δ

⁹<https://www.jawoollam.com/resources/ellipsometry-tutorial/ellipsometry-measurements>

are functions of the wavelength:

$$\frac{r_p}{r_s} = \tan(\Psi)e^{i\Delta} \quad (17)$$

The measurement can be repeated at different incidence angles. An exemplary measured dataset is plotted in figure 33 which was fitted by the software *EaseUS*, giving the following parameters:

- thickness $d = (1297 \pm 1) \text{ nm}$
- roughness $= (4.9 \pm 0.1) \text{ nm}$
- index of refraction $n(\lambda/\mu\text{m}) = 1.500 + 0.0050\lambda^{-2} + 0.000001\lambda^{-4}$

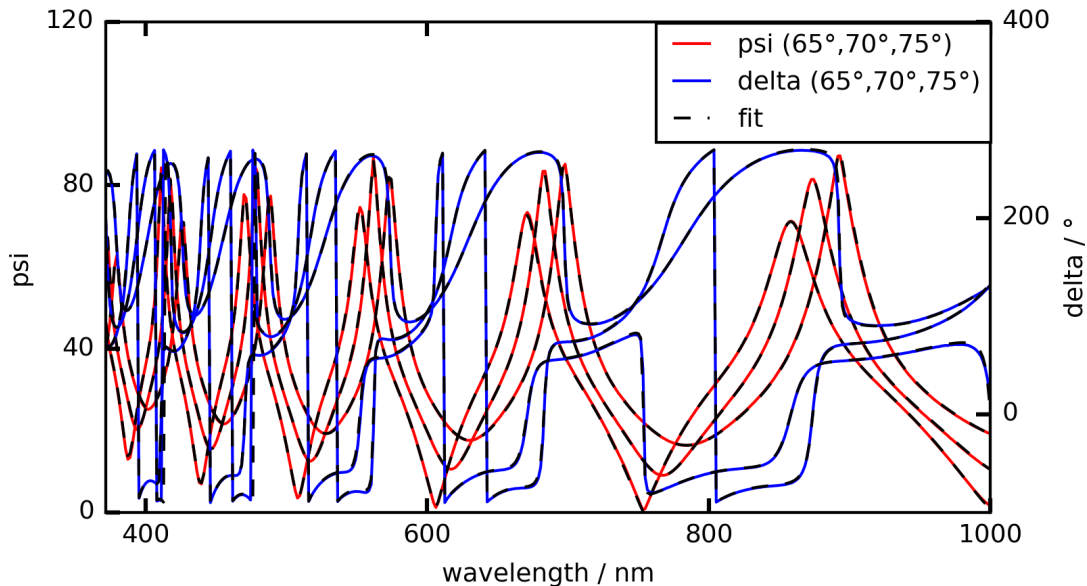


Figure 33: Exemplary ellipsometry measurement including fit

6.4 Initiated chemical vapour deposition

Initiated chemical vapour deposition (iCVD) is used in this work to deposit the custom ionomers onto various substrates. The reactor is shown in figure 34. The main part is the vacuum chamber with a glass cover evacuated by the rotary vane pump (PFEIFFER DUO65) to a base pressure of about 1 mTorr. Chemical jars at the left are heated to controlled temperatures and connected to the reactor via lines with needle valves. The lines are heated to about 100 °C to avoid condensation. The valves are used to control the flow-rate of the

evaporated chemicals flowing into the reactor. The flow-rate is measured by the increase in pressure over time when the main valve between reactor and pump is closed. A filament is heated inside the reactor to break apart the initiator molecules and to start the polymerization process. A laser is headed through the glass cover onto a piece of a Si wafer and reflected back into a detector measuring intensity over time. The growing polymer on the Si gives rise to an oscillating intensity at the detector as shown in figure 35. Considering the index of refraction of about 1.5, the incident angle of the laser of approximately 13° as well as the wavelength of the laser of 633 nm, the thickness of the polymer has to increase by approximately 200 nm to fit one more wavelength into the optical path and produce constructive interference again. Therefore, the current thickness of the layer can be read from the intensity versus time graph by counting gaps between maxima and multiplying by 200 nm, which in the case of figure 35 gives a thickness of about 1.86 μm . High accuracy is not necessary, because the thickness gets anyway measured after the depositions by the much more accurate ellipsometer.

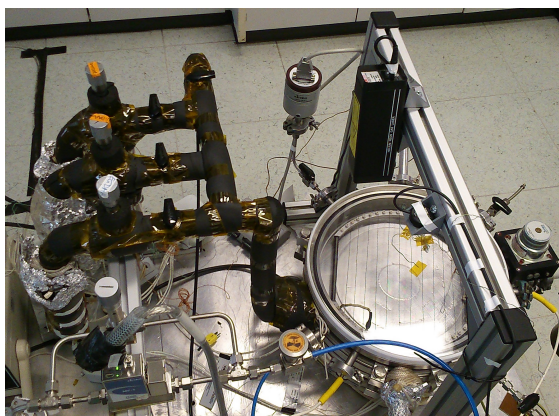


Figure 34: iCVD reactor

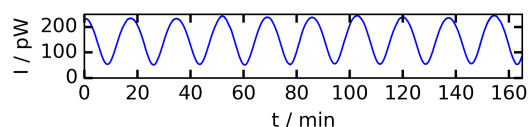


Figure 35: Exemplary laser intensity data for in-situ thickness measurement

6.5 Chemicals

The chemicals used for the iCVD process are the following:

- **Methacrylic acid (MAA):** This monomer has the functional carboxylic acid group providing the H^+ ion in the presence of H_2O turning the polymer into an ionomer, see figure 36a. The double-bond to the CH_2 group is broken in the polymerization process.

- **Ethylene glycol dimethacrylate (EGDMA):** This monomer is called cross-linker since it has double bonds at both ends cross-linking the resulting polymer, see figure 36b.
- **2-Hydroxyethyl methacrylate (HEMA):** HEMA is hydrophilic and leads to faster water uptake in the resulting polymer, see figure 36c.
- **Tert-butyl peroxide (TBPO):** TBPO is the initiator molecule (see figure 36d). Its labile O-O bond is broken by the filament in the iCVD reactor, thus radicals are produced initiating polymerization.
- **1H,1H,2H,2H-Perfluorodecyl acrylate (PFDA):** This monomer was used as hydrophobic backbone, see figure 36e.

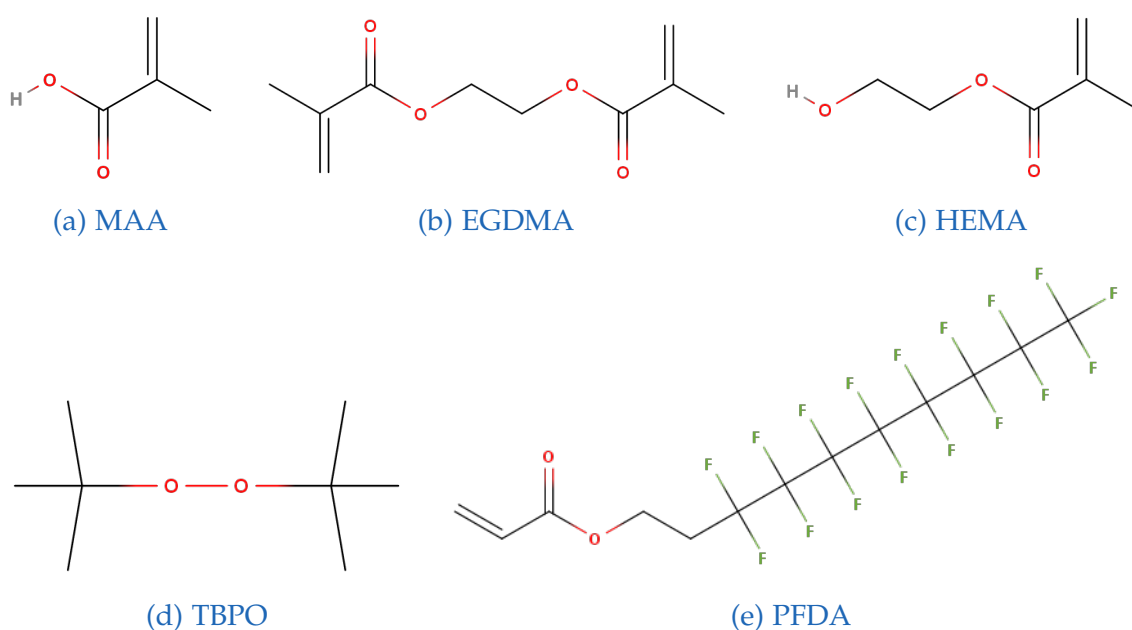


Figure 36: Chemical structures of monomers used for iCVD ¹⁰

6.6 Substrates and deposition conditions

The following substrates were used to deposit the custom ionomers on them:

- **Square pieces of a Si wafer:** This substrate is well suited for investigations of the ionomers since it allows FTIR transmission measurements and ellipsometry due to the very smooth surface
- **Polyethylene naphthalate (PEN):** 100 μm thick substrate with a smooth surface.

¹⁰The figures were exported from <http://molview.org/>

- **Polytetrafluoroethylene (PTFE, Teflon):** This 63 μm thick substrate is 84 % porous and the idea was to fill the pores (pore-size 0.45 μm) with ionomers and use the substrate as reinforcement.
- **Custom PCB from Eurocircuits**

At the beginning of this thesis, the PEN and PTFE substrates which are flexible were used to deposit series 1 and 2 of custom ionomers on them and the plan was to use the clamp to measure conductivity. Since the manual connection process of the $\sim 1 \mu\text{m}$ thick ionomers to the platinum wires turned out to be too crude, the fourth substrate, the PCB (as discussed in section 6.1), was used for two further series (series 3 and 4) of depositions. For completeness, the deposition conditions for series 1 and 2 are listed in the appendix 10.1. Series 3 was deposited using MAA and EGDMA. The idea was to use MAA since this monomer provides the conductive ions and to use EGDMA as cross linker to make it stable in water. The volume fraction of EGDMA was varied as shown in figure 37 and the individual deposition conditions and properties are listed in table 3.

The working pressure was set to 350 mTorr. The MAA jar temperature was 70 $^{\circ}\text{C}$ and the EGDMA jar temperature was 80 $^{\circ}\text{C}$. The heating current was 1.3 A which gave rise to a filament temperature of 313 $^{\circ}\text{C}$. The substrate temperature was set to 24 $^{\circ}\text{C}$ and measured to be 25 $^{\circ}\text{C}$.

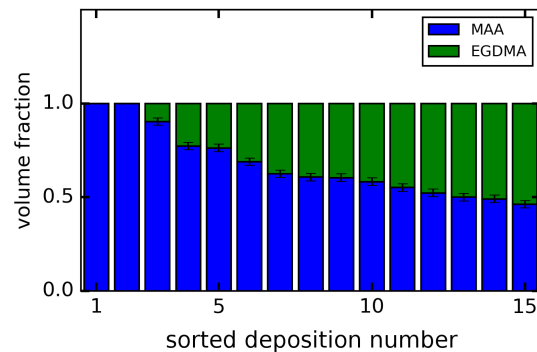


Figure 37: Volume fractions of p-MAA-EGDMA series

Deposition 18 had to be discarded since MAA polymerized inside the jar during deposition. Deposition 27 and 28 lead to polymers soluble in water.

Probably the chain length was too short or the number of cross-links too small. The same is true for deposition 11, 12, 13 and 19. Deposition 28 was performed using 12 samples simultaneously at different locations in the reactor as shown in figure 38 to investigate spatial variations.

Table 3: Deposition parameters and properties of series 3

Bulk fraction was measured with FTIR with an error of about $\pm 5\%$

Thickness measured with ellipsometry with an error of about ± 10 nm

Abbreviations used: nvp for needle valve position, dep for deposition

	nvp / pt	flowrate / sccm				volume fraction		thickness	dep. rate
dep	EGDMA	MAA	EGDMA	TBPO	N2	MAA	EGDMA	nm	nm/min
11	0	3.00	0.00	0.80	3.7	1.00	0.00	2020	11.6
12	25	3.25	0.013	0.82	0	1.00	0.00	2174	10.3
13	50	2.62	0.035	0.73	0	0.90	0.10	1309	9.6
14	75	3.11	0.09	0.76	0	0.61	0.39	1297	14.4
15	100	2.43	0.122	0.695	1.5	0.46	0.54	1274	13.4
16	125	3.76	0.182	0.74	3	0.52	0.48	1290	8.3
17	87.5	4.08	0.162	0.855	1	0.50	0.50	1202	13.2
19	62.5	3.85	0.061	0.86	0	0.77	0.23	1258	11.7
20	80	4.6	0.14	0.79	0	0.60	0.40	1986	13.2
21	90	3.15	0.11	0.67	1	0.58	0.42	1274	11.0
22	75	3.6	0.08	0.63	0	0.49	0.51	1354	15.2
23	70	3.5	0.08	0.68	0	0.55	0.45	1377	15.5
24	55	4.4	0.08	0.86	0	0.62	0.38	990	12.4
25	40	3.9	0.06	0.68	0	0.76	0.24	1348	11.5
26	52	3.82	0.07	0.74	0	0.69	0.31	1218	13.5
27	150	4.17	0.34	0.72	5	0.84	0.16	1265	10.0
28_1	60	4.1	0.14	0.78	0	0.71	0.29	1277	10.6
28_2						0.69	0.31	1345	11.2
28_3						0.68	0.32	964	8.0
28_4						0.73	0.27	1332	11.1
28_5						0.73	0.27	1291	10.7
28_6						0.71	0.29	1034	8.6
28_7						0.74	0.26	1440	12.0
28_8						0.74	0.26	1398	11.6
28_9						0.76	0.24	1605	13.3
28_10						0.75	0.25	1596	13.3
28_11						0.71	0.29	1236	10.3
28_12						0.72	0.28	957	7.9
31_1	60	3.11	0.09	0.76	0	0.56	0.44	2037	12.0
31_2						0.58	0.42	2118	12.5
31_3						0.63	0.37	1961	11.6
31_4						0.64	0.36	2044	12.0
31_5						0.63	0.37	2258	13.3
31_6						0.64	0.36	2167	12.8

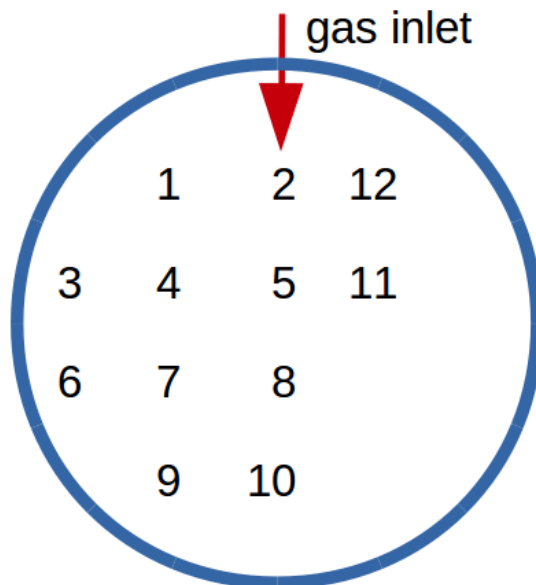


Figure 38: locations of dep28 samples in reactor

Series 4 was deposited by increasing the flow-rate of HEMA step by step. Depositions 29 and 32 contained 6 samples and depositions 33 and 34 contained 3 samples, which were positioned in the reactor in a line with the first sample being the closest to the gas inlet. The deposition conditions and parameters are listed in table 4, of which the volume fractions as well as the thicknesses, all with sample standard deviation, are calculated from the FTIR measurements on the single samples which are listed in table 5. The resulting volume fractions are plotted in figure 39. All other parameters such as filament temperature, working pressure and substrate temperature were the same as in series 3.

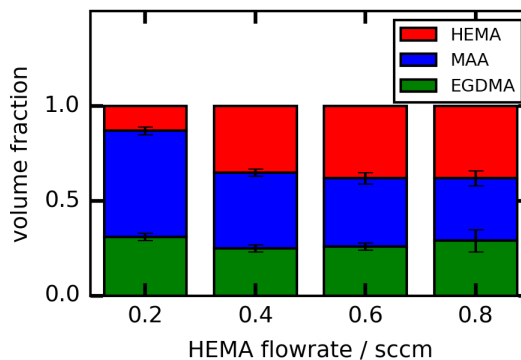


Figure 39: Volume fractions of p-MAA-EGDMA-HEMA series

Table 4: Deposition parameters and properties of series 4

Volume fraction and thickness values are averages and sample standard deviations are calculated using table 5.

dep	flowrate / sccm				volume fraction			thickness
	MAA	HEMA	EGDMA	TBPO	MAA	HEMA	EGDMA	nm
29	3.1	0.20	0.09	0.76	0.56 ± 0.02	0.13 ± 0.01	0.31 ± 0.02	1260 ± 100
32	3.2	0.41	0.085	0.76	0.40 ± 0.02	0.35 ± 0.02	0.25 ± 0.01	1350 ± 110
33	3.1	0.60	0.09	0.76	0.36 ± 0.02	0.38 ± 0.04	0.26 ± 0.02	1070 ± 220
34	3.1	0.82	0.09	0.76	0.33 ± 0.02	0.38 ± 0.06	0.29 ± 0.08	1020 ± 340

Table 5: Volume fractions and thicknesses of series 4 measured by FTIR

dep	volume fraction			thickness
	MAA	HEMA	EGDMA	nm
29_1	0.52	0.14	0.34	1247
29_2	0.55	0.13	0.33	1221
29_3	0.57	0.12	0.31	1160
29_4	0.58	0.11	0.30	1163
29_5	0.58	0.14	0.28	1315
29_6	0.55	0.14	0.30	1431
32_1	0.36	0.38	0.25	1509
32_2	0.39	0.35	0.26	1358
32_3	0.42	0.32	0.26	1222
32_4	0.41	0.33	0.26	1239
32_5	0.41	0.35	0.23	1440
32_6	0.42	0.34	0.24	1336
33_1	0.31	0.41	0.27	1432
33_2	0.36	0.38	0.26	1071
33_3	0.35	0.34	0.31	1049
34_1	0.32	0.44	0.24	1364
34_2	0.35	0.38	0.26	1003
34_3	0.31	0.31	0.38	679

7 Preliminary measurements

The impedance spectroscopy setup was new at the institute and therefore, some preliminary measurements were performed on deionized water as well as on the standard sample *Nafion* to test the setup as well as the data evaluation method.

7.1 Measurements of water

Deionized water still contains some ions, since parts of it dissociate ($\text{pH} \approx 7$) and additionally, impurities like CO_2 dissolves in it if it is exposed to air. The impedance of two electrodes immersed in water as shown in figure 40 can therefore be modeled with the equivalent circuit discussed in section 5.1.3. Figure 41 and 42 show the same measured data with a fit using equation 6 as well as the same model and fitting parameters but without constant phase element (using $P = 0$). The latter is just a parallel circuit of a resistor and a capacitor, which is an empirical non-physical model since it suggests a finite and real impedance at $\omega = 0$. In this case, the impedance maps the real number ω onto a perfect circle in the complex plane, labeled $Z(\omega)$. This circle has the property, that at the minimum of the imaginary part the frequency is given by

$$f_{\text{top}} = \frac{1}{2\pi RC} \quad (18)$$

This frequency is labeled f_{top} , since it is the frequency at which the impedance in the Nyquist plot is located at the top.

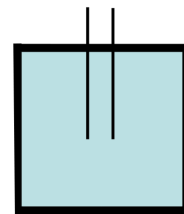


Figure 40: Two point water measurement setup

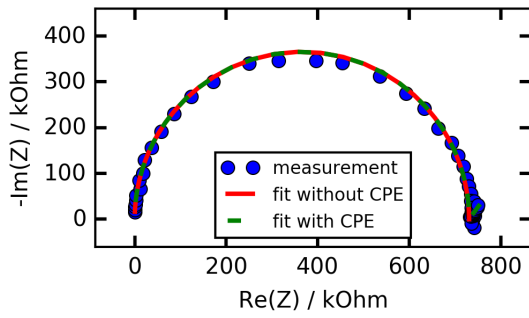


Figure 41: Bode plot of two point impedance spectroscopy measurement of deionized water fitted by equation 6

$$R = (731 \pm 4) \text{ k}\Omega$$

$$C = (9.68 \pm 0.06) \text{ pF}$$

$$P = (60 \pm 30) * 10^3 \Omega \text{ s}^{\frac{2\varphi}{\pi}}$$

$$\varphi = (-0.9 \pm 0.3) \text{ rad}$$

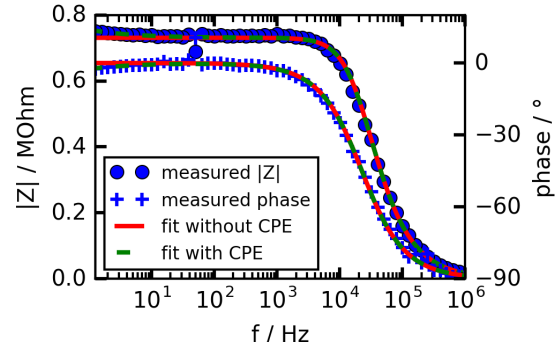


Figure 42: Nyquist plot of two point impedance spectroscopy measurement of deionized water (same data as in figure 41)

The presented equivalent circuit and its interpretation is suggested by the author and could be verified further by an experiment varying the distance between the electrodes. A hint in favor of the model is an estimation of the capacity of two electrodes immersed in water as dielectric. This estimation is very rough since the measurement was performed with two electrodes in the clamp filling the volume partly with *Teflon*. According to [13], the capacity of two parallel wires of length $l = 1 \text{ cm}$, radius $a = 0.5 \text{ mm}$ and distance $d = 4.3 \text{ mm}$ in an dielectric with a dielectric constant of $\epsilon = \epsilon_0 \epsilon_r = \epsilon_0 * 78$ is given by

$$C = \frac{\pi \epsilon l}{\text{arcosh}\left(\frac{d}{2a}\right)} \approx 10^{-11} \text{ F} \quad (19)$$

which is of the same order of magnitude as the fitted data in figure 41.

Compared to the derived impedance for water solutions in [14], the impedance as stated above is mathematically very similar and shares two important characteristics as shown in figure 43. First, the higher frequency part looks like a semicircle of a parallel circuit of resistor and capacitor and at lower frequencies the imaginary part

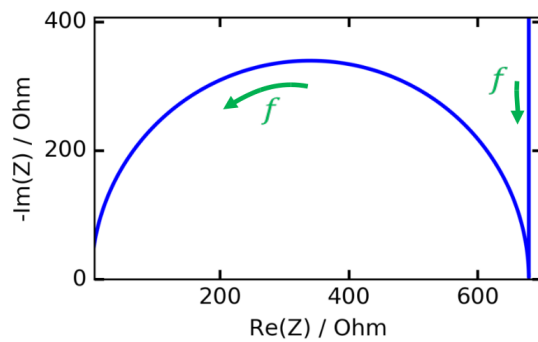


Figure 43: Nyquist plot of water solution impedance as derived in [14] using arbitrary parameters

of the impedance gets strongly negative. Second, the part of the curve where the semicircle crosses almost the real axis at low frequencies marks the resistance of the water.

7.2 Measurements on Nafion

*Nafion*TM is one of the state-of-the-art industrial proton conductive ionomers, trademark of *DuPont*. Its chemical structure is shown in figure 44. It has a fluorinated backbone and at the end of the side-groups is a sulphuric acid group. The conductivity of *Nafion* increases with the amount of absorbed water, since water ionizes the sulphuric acid groups. To get a maximum of conductivity, a rectangular piece of membrane was fixed in the clamp and immersed in deionized water.

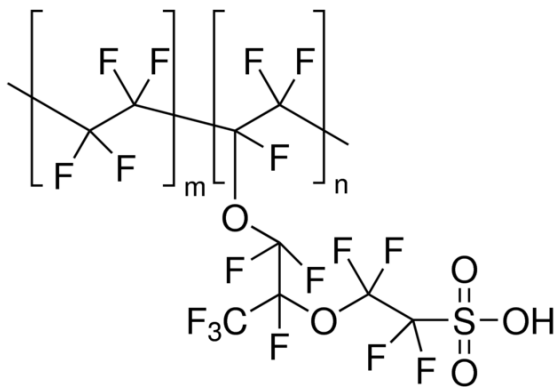


Figure 44: Chemical structure of *Nafion*¹¹

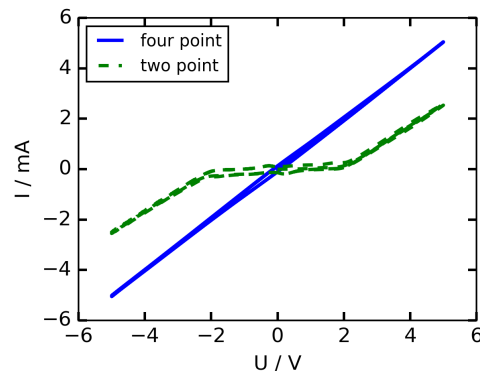


Figure 45: Direct current measurement of *Nafion* with clamp in water
sweep-rate = 500 mV/s
U ... voltage
I ... current

Figure 45 shows the direct current measurement on *Nafion* for two point and four point measurements. The voltage is swept linearly and slowly up and down in a triangular shape and the current is measured. The two point measurement shows the non-linear behavior due to the interfaces to the ionomer. For small voltages, almost no current is flowing and the interface behaves like a capacitor.

¹¹<http://www.sigmaaldrich.com/catalog/product/aldrich/274674?lang=de®ion=AT>

¹² The four-point measurement is almost linear but shows a small hysteresis. Additionally, the chemistry at the current driving electrodes changes over time since electrochemical reactions occur at them. The size of the current carrying part between the voltage sensing electrodes in this case was $a = (10.8 \pm 0.4)$ mm, $b = (50.8 \pm 0.5)$ μm , $l = (4.3 \pm 0.2)$ mm in size. The conductivity of *Nafion* is therefore

$$\sigma = \frac{l}{RA} = (81 \pm 1) \text{ mS cm}^{-1} \quad (20)$$

A two point impedance spectroscopy measurement of *Nafion* immersed in water was performed and fitted with equation 6. The data and the fit are shown in figure 46 and 47.

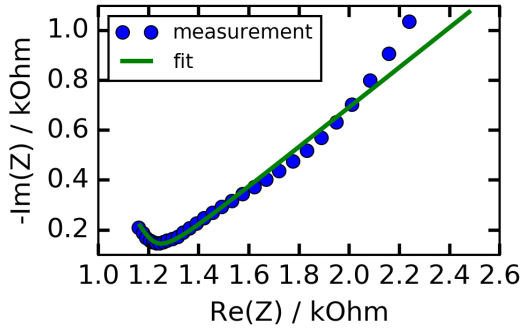


Figure 46: Nyquist plot of two point impedance spectrum of *Nafion* in H_2O , fit:

$$R = (1135 \pm 17) \Omega$$

$$C = (18 \pm 2) \text{ pF}$$

$$P = (36 \pm 3) 10^3 \Omega \text{ s}^{\frac{\pi}{2\varphi}}$$

$$\varphi = (-0.67 \pm 0.02) \text{ rad}$$

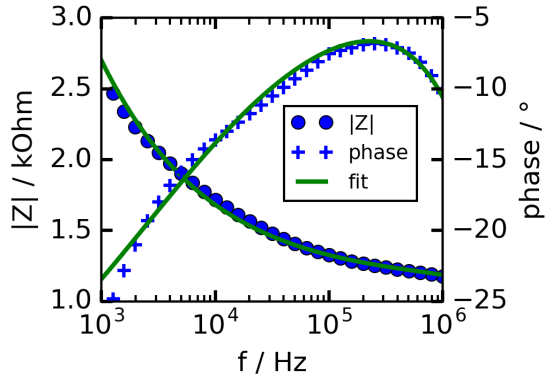


Figure 47: Bode plot of two point impedance spectrum of *Nafion* in H_2O , same data as in figure 46

The frequency f_{top} (as given in equation 18) is in this case

$$f_{\text{top}} = \frac{1}{2\pi RC} = 7.8 \text{ MHz} \quad (21)$$

which is well outside the maximum frequency of the Gamry Potentiostat of 1 MHz. Therefore, the Nyquist plot in figure 46 contains only part of the semicircle

¹²The increase of current in the two point measurement at about two volts can not directly be attributed to one of the two interfaces. This problem is solved in *Electrochemistry* by using a third electrode, the reference electrode, where the properties of one interface is studied. The reference electrode is able to keep an arbitrarily defined but constant potential difference between electrolyte and itself.

at high frequencies. At low frequencies, the model does not fit the data very well, which is most likely due to the idealized contact impedance.

A four point impedance spectroscopy measurement was performed and repeated after 10 minutes on a smaller frequency range, see figure 48. The magnitude of the impedance $|Z|$ in the frequency range between 1 to 10^5 Hz is about $1.1 \text{ k}\Omega$ and the phase is approximately zero. Therefore, the impedance acts as an ohmic resistor within this range whereas outside, this assumption is wrong. Figure 49 shows two similar measurements using 100 % humidity and $a = (10.0 \pm 0.5) \text{ mm}$. Both four point as well as the two point impedance spectroscopy measurements give the same conductivity of

$$\sigma = \frac{l}{R_{tw}} = (71.2 \pm 0.8) \text{ mS cm}^{-1} \quad (22)$$

The discrepancy between the DC and AC measurements might come from a different hydration state of *Nafion*.

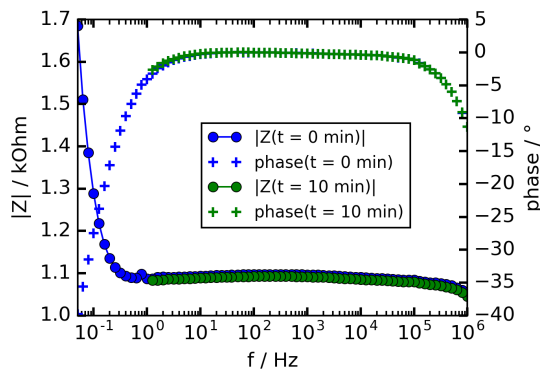


Figure 48: Impedance spectroscopy of *Nafion* with clamp in water

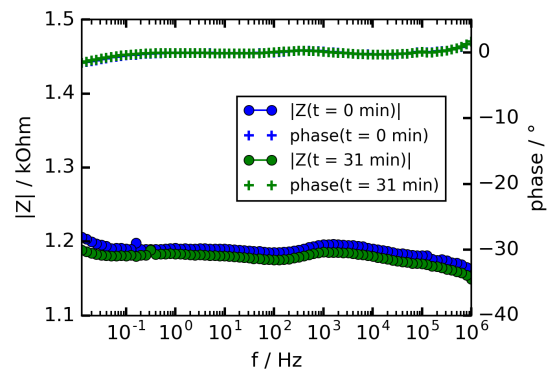


Figure 49: Impedance spectroscopy of *Nafion* with clamp in humidity

A two point through-plane impedance spectroscopy measurement was performed on *Nafion* using the through-plane measurement device (see figure 21). In through-plane direction, the ohmic resistance between the electrodes is much smaller than in the in-plane measurement due to the different geometry. The contact impedance in this case should be modified by an

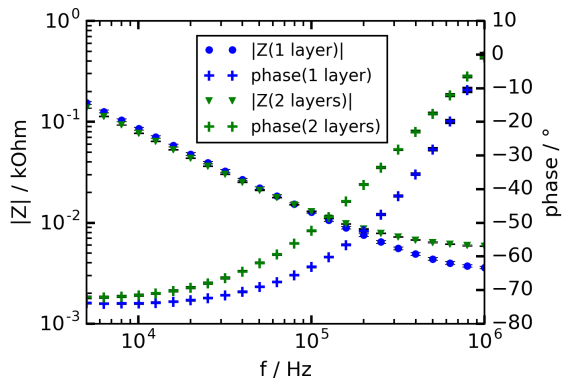


Figure 50: *Nafion* throughplane impedance spectrum

ohmic resistance in series to the constant phase element, which was ignored in the in-plane case due to its small value. To eliminate this ohmic contact resistance, two measurements were performed, first with one layer of *Nafion* and then with two layers, as shown in figure 50. These ohmic resistance values were subtracted and the conductivity of *Nafion* was calculated:

$$\sigma = \frac{l}{(R_2 - R_1)A} = (70 \pm 9) \text{ mS cm}^{-1} \quad (23)$$

8 Results

8.1 Swelling behavior investigated by spectroscopic ellipsometry

In situ swelling experiments using the temperature stage of the ellipsometer allowed to determine the swelling factor s defined as

$$s = \frac{d_2}{d_1} \quad (24)$$

where d_2 is the layer thickness after equilibration in air of 88% relative humidity and d_1 is the layer thickness before the equilibration at ambient relative humidity of 20%, given by the constraints of the experimental setup. A typical experimental data set is plotted in figure 51. The humidified air was generated by a bubbler and pumped into the temperature stage, containing an SHT15 humidity and temperature sensor. The equilibration took very long, almost one hour, and led to a swelling factor of $s = 1.07$. This experiment was performed for all samples listed in table 6, of which the results are shown in figure 52. The more MAA is in the layer, the bigger the swelling factor due to the hydrophilicity of MAA.

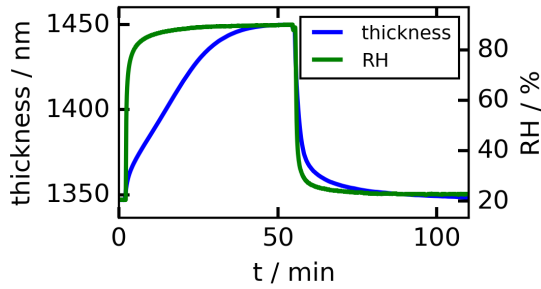


Figure 51: Swelling experiment of p-MAA-EGDMA layer on Si wafer (dep14)

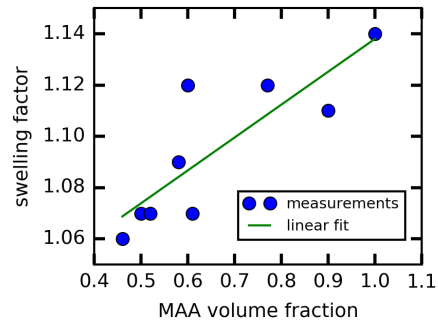


Figure 52: Swelling factor of p-MAA-EGDMA samples as a function of MAA volume fraction

Table 6: Swelling data of p-MAA-EGDMA on Si wafer

dep	MAA bulk fraction	swelling (88%RH)
12	1.00	1.14
13	0.90	1.11
14	0.61	1.07
15	0.46	1.06
16	0.52	1.07
17	0.50	1.07
19	0.77	1.12
20	0.60	1.12
21	0.58	1.09

8.2 Impedance spectroscopy results of series 1 and 2

Deposition series 1 and 2 were deposited on PTFE and PEN, which were afterwards measured using the clamp in deionized water as discussed in section 6.6. An exemplary measurement of these is shown in figure 53. First, the resistance of deionized water without ionomer was measured, which gave a value of 200 k Ω . After inserting a custom ionomer, the resistance went down to about 45 k Ω , which would indicate a well conductive ionomer. This measurement was repeated for some time giving consistent values, but the reference measurement after removing the ionomer showed no change in resistance anymore, indicating conductive water. This behavior could indicate that the ionomer partly dissolved in the water. To check this hypothesis, FTIR measurements were performed on

the ionomers on Si before and after water treatment as shown in figure 54. The spectra measured before water treatment is the same within the measurement error compared to after water treatment. It is concluded that the amount of dissolved matter was enough to disturb the impedance measurement, but not enough to be visible in the FTIR spectrum.

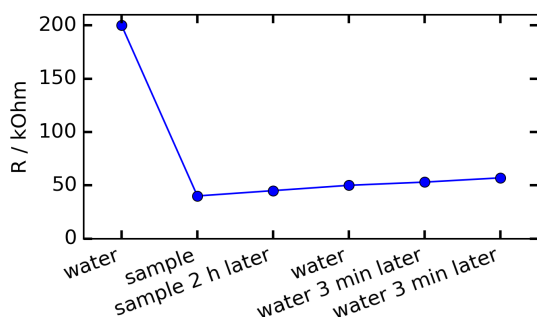


Figure 53: Exemplary measurement of thin custom ionomer with clamp in water

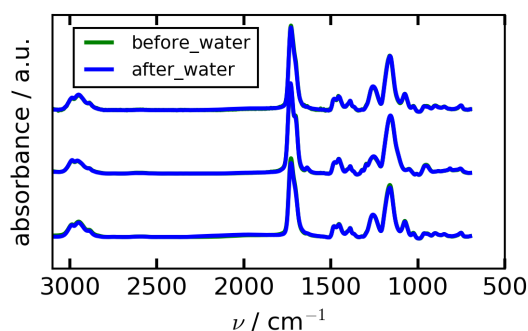


Figure 54: FTIR measurement before and after water treatment

8.3 Impedance spectroscopy results of series 3, p-MAA-EGDMA

Deposition series 3 was performed using PCB substrates. The conductivity was measured using 100 % relative humidity and a four point setup. The resistance decreases over time as the ionomer is taking up H₂O and converges to an equilibrated state. The conductivity values in the equilibrated state are listed in table 7.

Table 7: Conductivity values, series 3, relative error $\approx 40\%$

dep	11	12	13	14	15	16	17	19	20	21	22	23	24	25	26	31.1	31.2	31.3	31.4	31.5	31.6
$\sigma / \text{mS cm}^{-1}$	9.7	11	9.3	69	0.26	0.19	0.05	5.0	0.01	1.5	0.15	0.21	1.7	2.6	1.4	2.1	1.5	4.0	1.2	2.3	1.9

Dep31 was intended to reproduce dep14 since the latter showed very high conductivity. Six samples were coated at the same time, with the conditions of dep31. Their resistance over time is shown in figure 55.

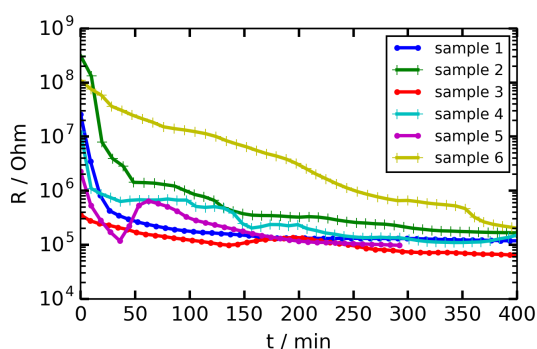


Figure 55: Resistance over time of all six PCBs of dep31

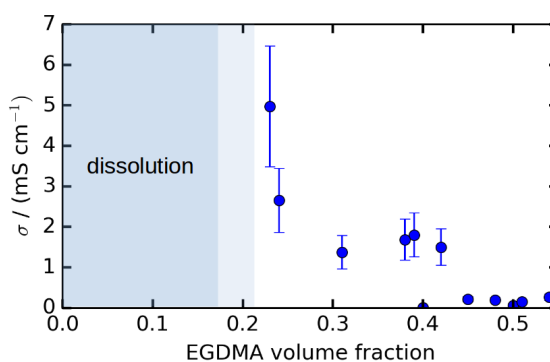


Figure 56: Conductivity of series 3, p-MAA-EGDMA, as a function of EGDMA fraction

This figure shows that the conductivity variations among the six replica is quite big even though the MAA volume fraction and therefore the acid group concentration is very similar (see table 3). This might come from the different channel geometries providing different amounts of available acid groups. Since all six samples of deposition 31 showed much lower conductivity values than deposition 14, the latter is regarded as outlier. The resistances of the dep31 samples in the steady state were used to calculate a conductivity of $\sigma = (1.8 \pm 0.6)$ mS/cm. The uncertainty on the conductivity value is relatively small. This is because the difference among the resistances of the samples decreased with time.

The conductivity values of deposition series 3 are plotted in figure 56 as a function of EGDMA volume fraction. Below an EGDMA volume fraction of about 0.2, the ionomers are not stable in water, marked by the blue region. For increasing EGDMA volume fraction, the conductivity goes down to zero as expected, since pure p-EGDMA does not conduct. An EGDMA volume fraction of about 0.4 seems to be a good compromise between stability and conductivity.

An exemplary two point impedance spectrum of dep33.3 using 100 % relative humidity is shown in figure 57 and 58 containing a fit with a model similar to figure 8 but with an additional charge transfer resistance parallel to the CPE. This measurement was performed in the equilibrated state.

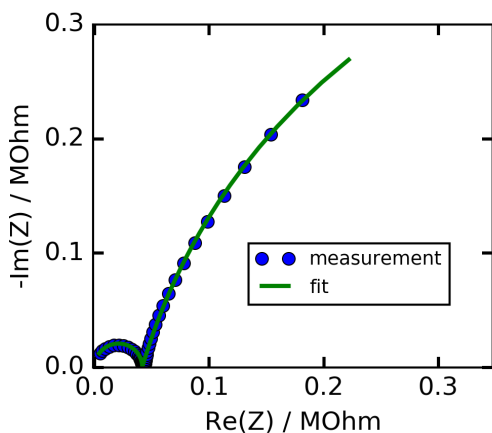


Figure 57: Exemplary Nyquist plot of custom ionomer two point impedance spectrum on PCB in humidity (dep33)

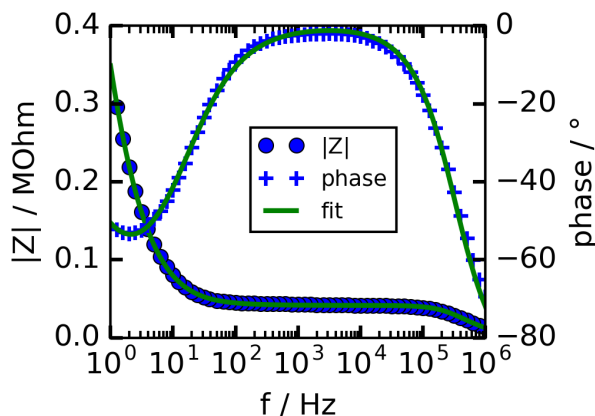


Figure 58: Bode plot of the same data shown in figure 57

An exemplary multi-distance measurement of a p-MAA-EGDMA sample (dep31_1) is shown in figure 59. Starting from a distance of 2 mm, the measurements show lower resistance than one would expect at first, but this is a systematic deviation resulting from the measurement across an ionomer volume with one or more unconnected electrodes in between. An unconnected electrode shortens a part of the length of the ionomer leading to lower resistance. This systematic error could in principle be corrected, but the magnitude of this error is well below the sample spread (as shown in figure 55) and can therefore be neglected.

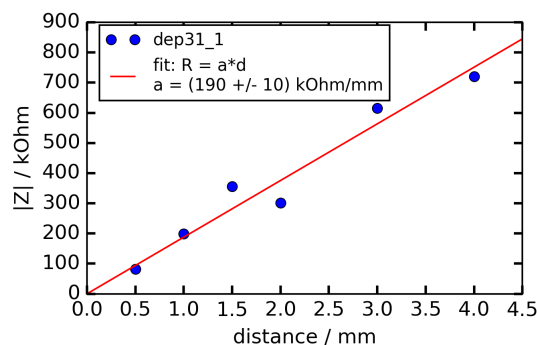


Figure 59: Exemplary multi distance impedance spectroscopy measurement of p-MAA-EGDMA sample (dep31.1)

8.4 Thickness and volume fraction variations in iCVD reactor of p-MAA-EGDMA, deposition 28 of series 3

The spatial variations inside the iCVD reactor were measured from samples of deposition 28 and are listed in table 3. The samples dep28.01 to dep28.10 were

located directly at the bottom of the reactor at different positions. The spatial dependence of the thickness is plotted in figure 60 and the EGDMA volume fraction dependence is plotted in figure 61. The overall effect is a decrease in EGDMA volume fraction further away from the gas inlet, which is most likely due to the bigger and less volatile molecule compared to MAA. An increase in thickness further away from the gas inlet is observed. Sample dep28_11 was lifted at one edge by a tape to about 0.1 mm to see the effect of an air gap below the Si wafer. The air gap had no significant effect on thickness and EGDMA fraction. Sample dep28_12 was placed on top of a PCB which increases its temperature due to the temperature gradient between chilled reactor bottom and heating wires above. The thickness of this sample was measured to be (960 ± 10) nm which is significantly less than the thickness of sample dep28_2 located next to it of (1345 ± 10) nm. The EGDMA fraction was the same compared to dep28.2 within the uncertainty of the measurements.

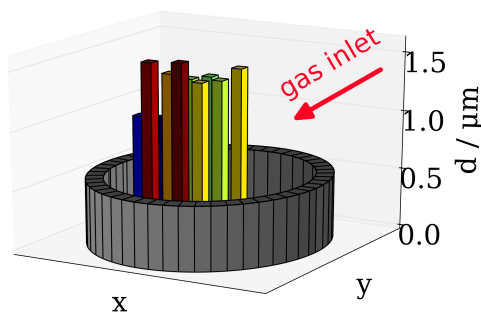


Figure 60: Spatial thickness dependence in iCVD reactor (dep28)

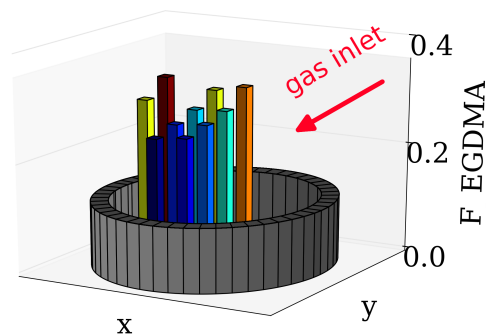


Figure 61: Spatial EGDMA volume fraction dependence in iCVD reactor (dep28)

8.5 Impedance spectroscopy results of series 4, p-MAA-EGDMA-HEMA

The resistance over time of series 4 is shown in figure 62. The errorbars were generated by the standard deviation on the conductivity measurements of the different replica of the same deposition. The equilibration was fitted using an exponential decay plus a constant. The equilibration time resulting from this fit is a measure of how fast the COOH groups are ionized in the presence of absorbed

H₂O and conductive channels are formed within the ionomer. This equilibration time is related to, but not the same as, the equilibration time measured by ellipsometry during the swelling process in humidity. The latter describes the rapidity of the simpler process of H₂O absorbing in the ionomer and therefore increasing its thickness. Both equilibration times are plotted in figure 63. The equilibration time measured by ellipsometry decreases for increasing HEMA flow rate due to the hydrophilicity of HEMA. The equilibration time measured by impedance spectroscopy shows a similar behavior at the beginning, but increases for values bigger than 0.4 sccm. This might come from the larger number of microscopic configuration of water in the ionomer at high HEMA volume fractions. Figure 64 shows the conductivity of the five samples which is maximal at a HEMA flow rate of 0.4 sccm and has a value of $\sigma = (8 \pm 3)$ mS/cm.

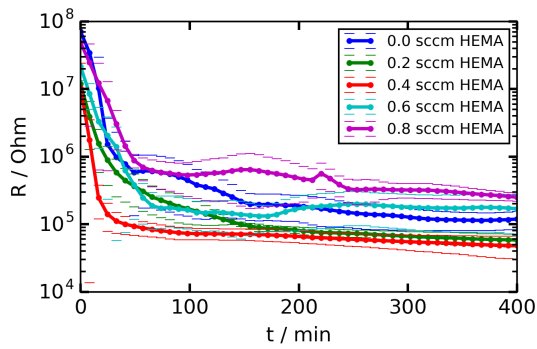


Figure 62: Resistance over time of series 4

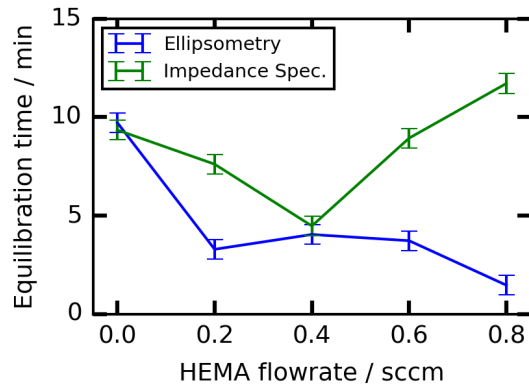


Figure 63: Equilibration times of series 4

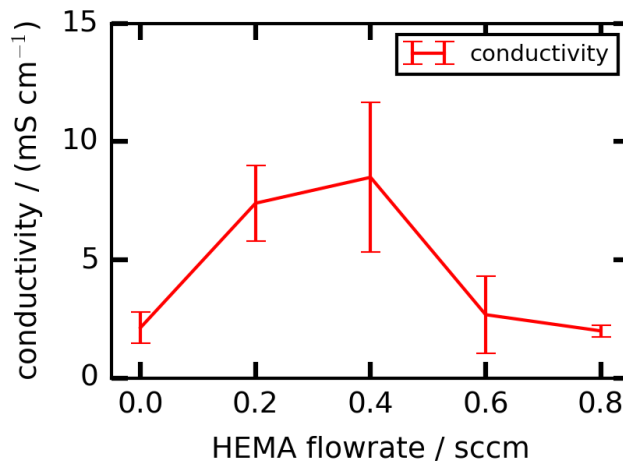


Figure 64: Conductivity of series 4

8.6 Results of morphologic investigations

Optical microscopy was used to investigate the cross-section of p-MAA-EGDMA on a PCB sample (dep20) to visualize the thickness of the layer and compare it to the thickness of a layer on the Si wafer measured by ellipsometry. The sample was encapsulated in resin, cut and grinded to make the cross-section visible. Figure 65 shows the cross-section at the largest possible scale available at the optical microscope (Olympus, BX51 TRF). The lower half shows the fiber reinforced PCB bulk material, on which the electrodes are located. The upper half shows the resin. By zooming in to an electrode at the smallest possible scale, figure 66 was recorded. In this image, the Ni layer of the ENIG coating on the Cu electrode is visible. Also the p-MAA-EGDMA layer is visible and an approximately equal thickness on the metal and on the PCB bulk material can be confirmed. By measuring the thickness of the layer in terms of number of pixels and using the length of the scale bar, the thickness was determined to be 1.9 μm , which agrees with the value measured by ellipsometry of 1.986 μm .

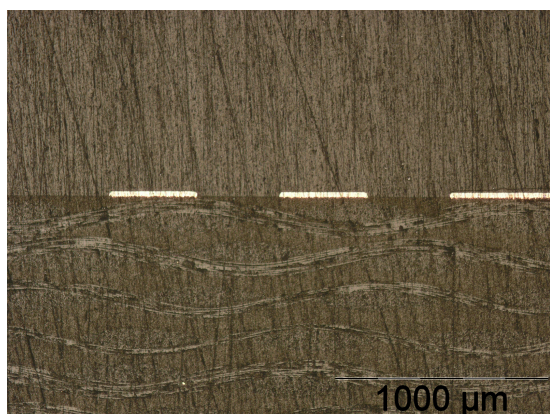


Figure 65: Optical microscopy image of p-MAA-EGDMA on PCB cross-section, dep20

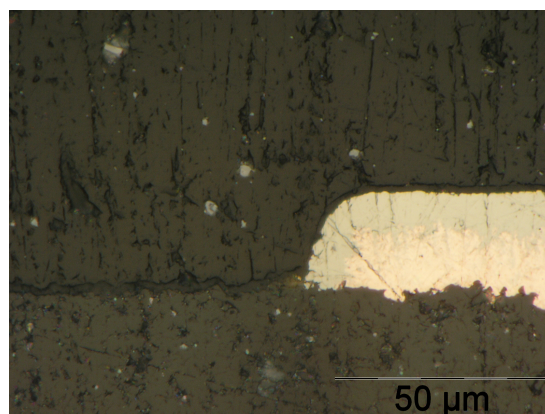


Figure 66: Optical microscopy image of p-MAA-EGDMA on PCB cross-section, dep20

The effect of liquid water on a p-MAA-EGDMA coated Si wafer (dep14) was investigated. Figure 67 shows a drop of water applied on top and some channels, which most likely are due to partly delamination of the layer from the smooth surface of the Si wafer. Figure 68 shows the same sample at another location.

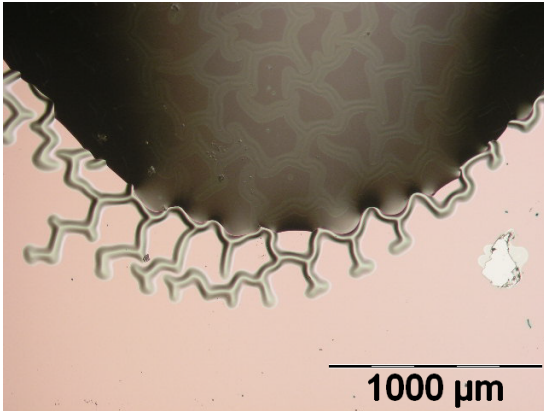


Figure 67: Optical microscopy image of p-MAA-EGDMA on Si with liquid water, dep14

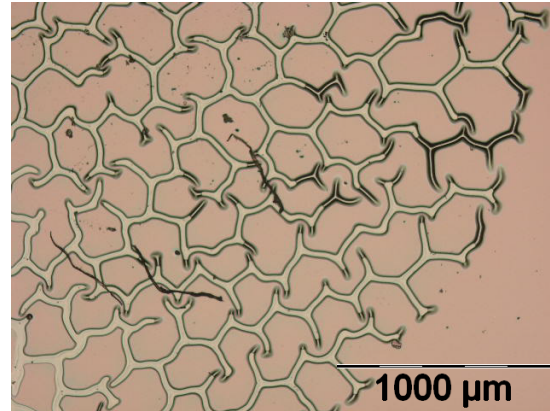


Figure 68: Optical microscopy image of p-MAA-EGDMA on Si with liquid water, dep14

Atomic force microscopy (AFM) was used to measure the surface morphology of the PCB bulk material. Figure 69 shows the AFM amplitude image and figure 70 shows the 3d topography image of the same data set. The images were plotted with the program *Gwyddion*¹³, which also calculates the RMS roughness, which in this case gives 0.39 μm. The same measurement was performed on a similar

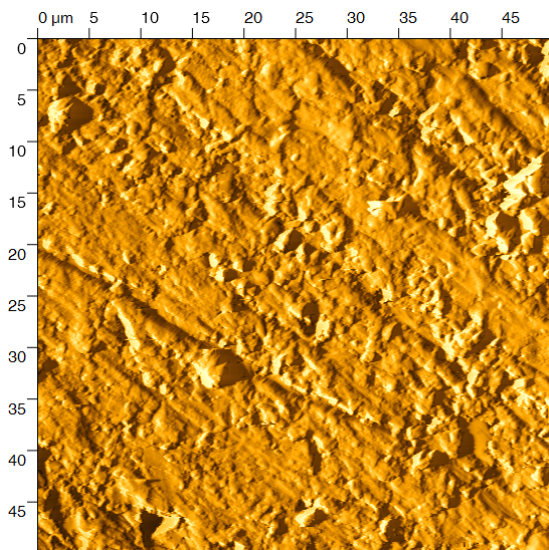


Figure 69: Atomic force microscopy amplitude image of PCB bulk material

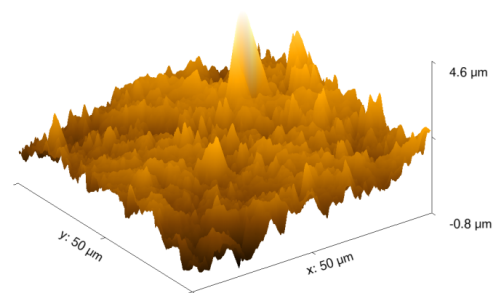


Figure 70: Atomic force microscopy 3d topography image of PCB bulk material

location after a p-MAA-EGDMA layer was deposited (dep14). Figure 71 shows the AFM amplitude image and figure 72 shows the 3d topography image of the

¹³<http://gwyddion.net/>

same data set. The RMS roughness in this case is $0.36\ \mu\text{m}$ which is a bit less than in the uncoated condition.

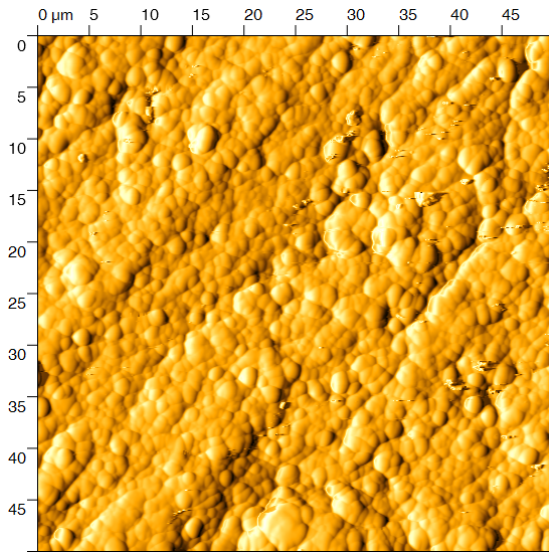


Figure 71: Atomic force microscopy amplitude image of p-MAA-EGDMA on PCB bulk material (dep14)

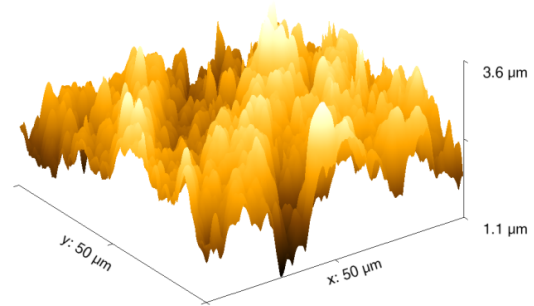


Figure 72: Atomic force microscopy 3d topography image of p-MAA-EGDMA layer on PCB bulk material (dep14)

Electron microscopy was used to investigate the p-MAA-EGDMA on PCB (dep14), see figure 73 and 74. The stresses in the polymer caused the ionomer layer to crack partly, especially on the electrodes where the layer does not adhere as well. This stresses are due to the evaporation of the adsorbed water caused by the vacuum of the electron microscopy chamber.

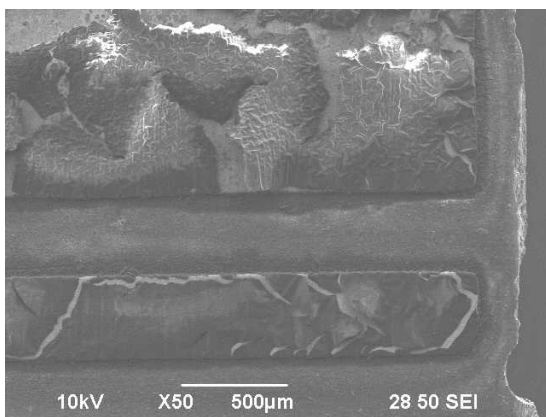


Figure 73: Secondary electron microscopy image of p-MAA-EGDMA on PCB (dep14)

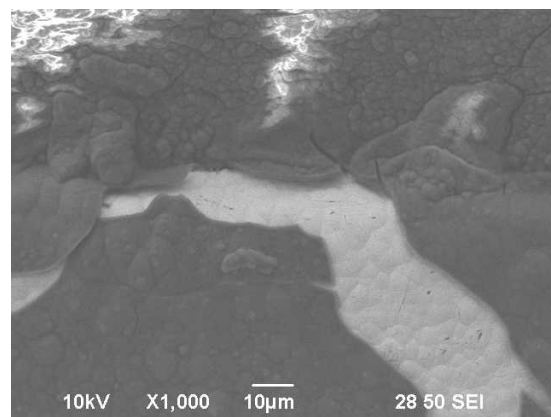


Figure 74: Secondary electron microscopy image of p-MAA-EGDMA on PCB (dep14), zoomed in

8.7 Results of X-Ray experiments

An X-Ray diffraction (XRD) experiment was performed on a p-MAA-PFDA sample (dep04) as well as on a p-MAA-EGDMA sample (dep14). For both the ionomer deposited on the Si wafer was used. The measurement was performed in specular conditions, in which the detector is positioned such that the angle of incidence equals the measured angle of reflection. The intensity is recorded as a function of incidence angle θ and shown in figure 75. The p-PFDA-MAA sample shows a Bragg-peak at about $\theta = 8.3^\circ$, from which a periodicity of length d in the electron density normal to the surface can be calculated:

$$d = \frac{\lambda}{2\sin(\theta)} = (5.3 \pm 0.3) \text{ \AA} \quad (25)$$

where λ is the wavelength of Cu K-alpha of about 1.54 \AA . The periodicity in the electron density is due to some crystalline arrangement within the ionomer. The peak at $\theta = 16.5^\circ$ is due to the Si substrate and therefore does not contain information about the ionomer. The XRD spectrum of the p-MAA-EGDMA sample does not contain any Bragg peak due to the ionomer and therefore the ionomer does not contain crystalline domains.

The same experiment was performed at very small angles, which is then called X-Ray Reflectivity, see figure 76.

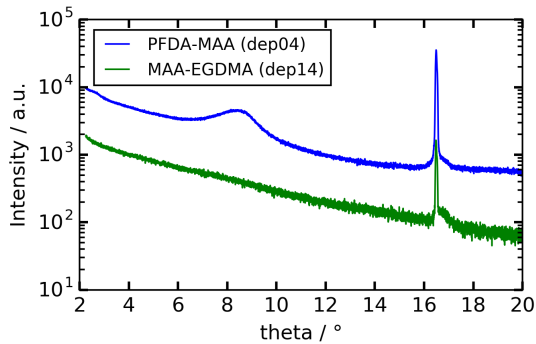


Figure 75: X-Ray diffraction experiment on p-MAA-PFDA (dep04) and p-MAA-EGDMA sample (dep14)

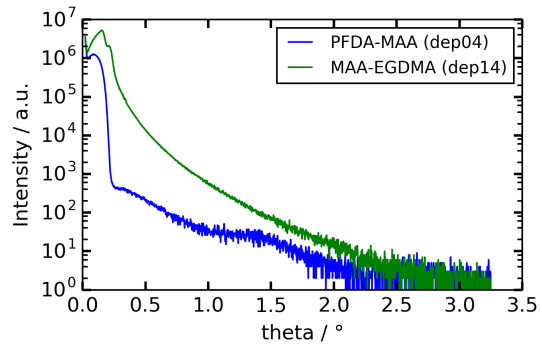


Figure 76: X-Ray reflectivity experiment on p-MAA-PFDA (dep04) and p-MAA-EGDMA sample (dep14)

9 Conclusions

The conductivity of the 50 μm thick standard sample *Nafion* was measured without difficulty in humidity as well as water, in-plane and through-plane due to its high conductivity of about 70 to 80 mS/cm at room temperature. Two point impedance spectroscopy measurements gave the most insight into the setup comprising of *Nafion* and clamp due to a good fit of a model to the spectrum (see figure 47). Four point impedance spectroscopy was useful to measure the conductivity only, since the contact influence is almost eliminated. The measurement of the custom ionomers turned out to be more difficult since their thickness is thinner by about a factor of 40 and also less conductive, again by a factor of about 40, which increases the influence of the surrounding medium. In case of water as surrounding medium the conductivity was not determinable at all since small amounts of impurities in the water already conduct as much as the ionomer itself and therefore humidity had to be used. Additionally, the contacts at the beginning were made manually using the clamp which partly destroyed the ionomer. This problem was solved by directly depositing the ionomer onto electrodes avoiding manual connection problems. For a p-MAA-EGDMA series with increasing EGDMA volume fraction, a good compromise between stability and conductivity was found at about 0.4 EGDMA volume fraction showing a conductivity of $\sigma = (1.8 \pm 0.6)$ mS/cm (dep31). By adding HEMA which is hydrophilic, the conductivity increased and the swelling time decreased (figure 64 and 63). The maximum conductivity was found to be $\sigma = (8 \pm 3)$ mS/cm for an ionomer (dep32) of volume fractions of 0.40 ± 0.02 MAA, 0.35 ± 0.02 HEMA and 0.25 ± 0.01 EGDMA.

References

- [1] Christopher M. Evans et al. "Anhydrous Proton Transport in Polymerized Ionic Liquid Block Copolymers: Roles of Block Length, Ionic Content, and Confinement." In: *Macromolecules* 49.1 (2016), pp. 395–404. DOI: [10.1021/acs.macromol.5b02202](https://doi.org/10.1021/acs.macromol.5b02202). eprint: <http://dx.doi.org/10.1021/acs.macromol.5b02202>. URL: <http://dx.doi.org/10.1021/acs.macromol.5b02202> (cit. on p. 8).

- [2] Han Gao and Keryn Lian. "Proton-conducting polymer electrolytes and their applications in solid supercapacitors: a review." In: *RSC Adv.* 4 (62 2014), pp. 33091–33113. DOI: [10.1039/C4RA05151C](https://doi.org/10.1039/C4RA05151C). URL: <http://dx.doi.org/10.1039/C4RA05151C> (cit. on pp. 8, 17).
- [3] Christian Ranacher et al. "Layered Nanostructures in Proton Conductive Polymers Obtained by Initiated Chemical Vapor Deposition." In: *Macromolecules* 48.17 (2015), pp. 6177–6185. DOI: [10.1021/acs.macromol.5b01145](https://doi.org/10.1021/acs.macromol.5b01145). eprint: <http://dx.doi.org/10.1021/acs.macromol.5b01145>. URL: <http://dx.doi.org/10.1021/acs.macromol.5b01145> (cit. on pp. 8, 9).
- [4] Anna Maria Coclite et al. "Novel hybrid fluoro-carboxylated copolymers deposited by initiated chemical vapor deposition as protonic membranes." In: *Polymer* 54.1 (2013), pp. 24–30 (cit. on p. 9).
- [5] J. M. Rubi and S. Kjelstrup. "Mesoscopic Nonequilibrium Thermodynamics Gives the Same Thermodynamic Basis to Butler-Volmer and Nernst Equations." In: *The Journal of Physical Chemistry B* 107.48 (2003), pp. 13471–13477. DOI: [10.1021/jp030572g](https://doi.org/10.1021/jp030572g). eprint: <http://dx.doi.org/10.1021/jp030572g>. URL: <http://dx.doi.org/10.1021/jp030572g> (cit. on p. 11).
- [6] Jean Jacquelin. "The Phasance concept: a review." In: *Current Topics in Electrochemistry* 4 (1997). <https://www.scribd.com/doc/71923015/The-Phasance-Concept>, pp. 127–136. URL: <http://www.researchtrends.net/tia/abstract.asp?in=0&vn=4&tid=19&aid=4474&pub=1997&type=3> (cit. on p. 13).
- [7] James Ross MacDonald. "Impedance Spectroscopy—Emphasizing Solid Materials and Systems." In: *Wiley-Interscience, John Wiley and Sons*, (1987), pp. 1–346 (cit. on p. 14).
- [8] P. Atkins and J. de Paula. *Physical Chemistry*. W. H. Freeman, 2006. ISBN: 0-7167-8759-8. URL: <https://chemistry.com.pk/books/atkins-physical-chemistry/> (cit. on p. 15).
- [9] Karen K. Gleason. "Overview of Chemically Vapor Deposited (CVD) Polymers." In: *CVD Polymers*. Wiley-VCH Verlag GmbH & Co. KGaA, 2015, pp. 1–11. ISBN: 9783527690275. DOI: [10.1002/9783527690275.ch1](https://doi.org/10.1002/9783527690275.ch1). URL: <http://dx.doi.org/10.1002/9783527690275.ch1> (cit. on pp. 17, 18).

- [10] Zyun Siroma et al. "Proton conductivity along interface in thin cast film of Nafion®." In: *Electrochemistry communications* 4.2 (2002), pp. 143–145 (cit. on p. 20).
- [11] Karpenko-Jereb L. Reiter V. Grampp G. "Development of methods to measure conductivity and osmotic drag of proton exchange membranes." In: *7th Int Summer School. Advanced Studies of Polymer Electrolyte Fuel Cells* (), pp. 143–144 (cit. on p. 20).
- [12] P. Buehlmann E. Pretsch and M. Badertscher. "Spektroskopische Daten zur Strukturaufklaerung organischer Verbindungen." In: (2010) (cit. on p. 23).
- [13] J.C. Slater and N.H. Frank. *Electromagnetism*. Dover Books on Physics. Dover Publications, 2012. ISBN: 9780486150406. URL: <https://books.google.at/books?id=hsDDAgAAQBAJ> (cit. on p. 35).
- [14] M. Becchi et al. "Impedance Spectroscopy of Water Solutions: The Role of Ions at the Liquid-Electrode Interface." In: *The Journal of Physical Chemistry B* 109.49 (2005). PMID: 16375317, pp. 23444–23449. DOI: [10.1021/jp044443r](https://doi.org/10.1021/jp044443r). eprint: <http://dx.doi.org/10.1021/jp044443r>. URL: <http://dx.doi.org/10.1021/jp044443r> (cit. on p. 35).
- [15] Anna Maria Coclite et al. "Novel hybrid fluoro-carboxylated copolymers deposited by initiated chemical vapor deposition as protonic membranes." In: *Polymer* 54.1 (2013), pp. 24–30. ISSN: 0032-3861. DOI: <http://dx.doi.org/10.1016/j.polymer.2012.11.004>. URL: <http://www.sciencedirect.com/science/article/pii/S0032386112009329> (cit. on p. 53).

10 Appendix

10.1 Desposition conditions of series 1 and 2

The deposition series 1 was performed using a working pressure of 800 mTorr and a heating current of 1.2 A which gave rise to a filament temperature of 313 °C. The temperature of the MAA jar was controlled to 70 °C, that of the PFDA jar to 80 °C and that of the TBPO jar was kept at room temperature of 24 °C. The parameters which changed from one deposition to the other are listed in table 8.

Table 8: Deposition parameters of series 1

dep	T _{set} °C	T _{measured} °C	flowrate / sccm				thickness nm	dep. rate nm / min	surface fraction / %	
			MAA	TBPO	N2	PFDA			MAA	PFDA
1	24	30	0.54	0.60	3.4	0.28	2600	31	8	92
2	24	30	1.09	0.59	3	0.13	2400	25	30	70
3	24	30	1.00	0.55	3.3	0.17	2000	22	21	79
4	24	30	0.47	0.60	3.3	0.13	2300	47	15	85
5	24	30	1.74	0.55	3.3	0.11	2100	19	40	60
6	50	55	1.00	1.02	3.6	0.3	1450	13	15	85

The series 2 was performed under the same conditions, but with a constant substrate temperature set to 20 °C and measured to be 24 °C, a heating current of 1.3 A and a working pressure of 350 mTorr. The parameters changing from deposition to deposition are listed in table 9. The surface fractions were calculated according to [15].

Table 9: Deposition parameters of series 2

dep	flowrate / sccm					thickness nm	dep. rate nm / min	surface fraction / %			swelling 1
	MAA	HEMA	EGDMA	TBPO	N2			MAA	HEMA	EGDMA	
7	3.00	0.65	0.092	0.79	3	1848	32	0.14	0.30	0.56	1.22
8	3.00	0.00	0.09	0.80	3.7	2040	13.7	0.21	0.00	0.79	1.05
9	3.03	0.62	0.083	0.83	3	2400	53.3	0.155	0.302	0.543	1.125
10	3.11	0.61	0.09	0.80	3	2000	43.6	0.155	0.285	0.562	

10.2 List of coding software

- Coding language: Python 3.5.1
- IDE: Spyder 2.3.9

10.3 Python scripts for FTIR measurements

```

1 # -*- coding: utf-8 -*-
2 """
3 Created on Tue Feb 16 10:42:19 2016
4
5 @author: Martin Tazreiter , tazreiter@student.tugraz.at
6 """
7
8 from __future__ import division
9
10 import pylab as plt

```

```

11 import os
12 import numpy as np
13 import tkinter
14 from tkinter import filedialog
15 import subprocess
16 import GeneralFunctions
17 from scipy import optimize

19 class FTIRfitter():
20     def __init__(self, folderpath_baselinecorrected, output_path=None, use_ATR = False,
21                 k_min = 1000.0, k_max = 2000.0, thickness_error_absolute = 1, # nm
22                 thickness_error_relative = 0.01, save_figure_and_data_flag = False,
23                 use_HEMA = True, minimum_volume_fraction_error=0.01):
24         self.output_path = output_path
25         self.folderpath_baselinecorrected = folderpath_baselinecorrected
26         self.use_ATR = use_ATR
27         self.k_min = k_min
28         self.k_max = k_max
29         self.thickness_error_absolute = thickness_error_absolute*(not self.use_ATR)
30         self.thickness_error_relative = thickness_error_relative
31         self.minimum_volume_fraction_error = minimum_volume_fraction_error
32         self.save_figure_and_data_flag = save_figure_and_data_flag
33         self.use_HEMA = use_HEMA
34         self.basis_functions_labels = ['EGDMA', 'MAA']
35         if self.use_HEMA:
36             self.basis_functions_labels.append('HEMA')
37         if self.use_ATR:
38             self.wavenumber, self.basis_functions = self.GetBasisFunctionsATR()
39         else:
40             self.wavenumber, self.basis_functions = self.GetBasisFunctionsTransmission()
41     def ReadFTIRdata(self, path): # absorbance spectra, thickness in nm
42         with open(path) as f:
43             lines = f.read().splitlines()
44             wavenumber_ = np.zeros(len(lines))
45             absorbance_ = np.zeros(len(lines))
46             for n, line in enumerate(lines):
47                 wavenumber_[n], absorbance_[n] = line.split()[0:2]
48             logical = np.logical_and(wavenumber_ > self.k_min, wavenumber_ < self.k_max)
49             wavenumber = wavenumber_[logical]
50             absorbance = absorbance_[logical]
51             return wavenumber, absorbance
52     def GetCoefficients(self, data): # basis_functions has to be a hstack of numpy
53         # vectors
54         basis_functions = np.vstack(self.basis_functions).transpose()
55         #x, residuals, rank, s = np.linalg.lstsq(basis_functions, data)
56         x, rnorm = optimize.nnls(basis_functions, data) # np.linalg.lstsq(basis_functions,
57         # data)
58         #X = np.dot(basis_functions.transpose(), basis_functions)
59         S = np.sum((np.dot(basis_functions, x) - data)**2)
60         n, m = basis_functions.shape
61         x_var = S / (n - m) * np.diag(np.linalg.inv(np.dot(basis_functions.transpose(),
62         basis_functions)))
63         return x, np.sqrt(x_var)
64     def CalculateSuperposition(self, path, wavenumber, A_data):

```

```

d_vec, sig_vec = self.GetCoefficients(A_data)
61 for k,d in enumerate(d_vec):
    print('d_{:s} = {:.2f}\n'.format(self.basis_functions_labels[k],d))
63 print('d = {:.2f}\n'.format(np.sum(d_vec)))
    d_error_vec = sig_vec + self.thickness_error_absolute + d_vec*self.
thickness_error_relative
65 F_vec = d_vec/np.sum(d_vec)
    F_error_vec = np.nan_to_num(F_vec*(d_error_vec/d_vec+np.sum(d_error_vec)/np.sum(
d_vec)))
67 F_error_vec = np.maximum(F_error_vec ,np.ones_like(F_error_vec)*0.01)
    parameters = F_vec, F_error_vec, d_vec, d_error_vec
69 return parameters
def PlotSuperposition(self ,wavenumber,A_data ,parameters ,data_name):
71 F_vec, F_error_vec, d_vec, d_error_vec = parameters
    plt.close()
73 if self.save_figure_and_data_flag:
        plt.ioff()
75 axis_font, legend_font = GeneralFunctions.GetFontsAndSetMPLproperties()
    fig = plt.figure(figsize=(12/2.54,8/2.54),dpi = 300)
77 ax0 = fig.add_subplot(111)
    plt.locator_params(nbins=4)
79 #dep28_x = '-'.join(os.path.splitext(os.path.split(1)[1])[0].split('-')[0:2])
    d_um = np.sum(d_vec)/1000 # in um
81 ax0.plot(wavenumber,A_data/d_um,linewidth = 2,label=data_name)#dep28_x)
    for k,d,i in enumerate(d_vec):
83         if self.use_ATR:
            label = 'fit: ' + self.basis_functions_labels[k]
85         else:
            label = 'fit: d_{:s} = '.format(self.basis_functions_labels[k]) +
GeneralFunctions.GetErrorString(d,i,d_error_vec[k]) + ' nm'
87         ax0.plot(wavenumber,d_i/d_um*self.basis_functions[k],'-',dashes=(3,3),label
= label,linewidth = 2)
            label_vec = []
89         if self.use_ATR:
            label_vec.append('')
91         else:
            label_vec.append('fit: d_sum = ' + GeneralFunctions.GetErrorString(np.sum(
d_vec),np.sum(d_error_vec)) + ' nm')
93         for k in range(len(self.basis_functions_labels)-1):
            label_vec.append('F({:s}) = '.format(self.basis_functions_labels[k]) +
GeneralFunctions.GetErrorString(F_vec[k],F_error_vec[k]))
95         ax0.plot(wavenumber,np.dot(d_vec,np.vstack(self.basis_functions))/d_um,'k--',
dashes=(5,5),label = '\n'.join(label_vec),linewidth = 2)
            ax0.set_xlabel('wavenumber / cm$^{-1}$')
97         if self.use_ATR:
            ax0.set_ylabel('absorbance / a.u.')
99         ax0.set_yticks([0])
        else:
101         ax0.set_ylabel('absorbance*d_sum$^{-1}$ / $\mu$m$^{-1}$')
    y_max = np.max(A_data)/d_um
103 ax0.set_ylim([-0.1*y_max,y_max*1.1])
    legend = ax0.legend(loc=(0.45,0.6),prop=legend_font)
105 legend.draggable(True)
    ax0.invert_xaxis()

```

```

107     #ax0.set_yticks([0])
108     if self.save_figure_and_data_flag:
109         if not os.path.exists(self.output_path):
110             os.makedirs(self.output_path)
111         plt.savefig(self.output_path + 'FTIR_' + data_name + '.png')
112 def GetBasisFunction(self, path, thickness): # thickness in mm
113     wavenumber, absorbance = self.ReadFTIRdata(path)
114     return wavenumber, absorbance/thickness # normalized by thickness
115 def GetBasisFunctionsTransmission(self):
116     basis_functions = [None]*len(self.basis_functions_labels)
117     wavenum_vec = [None]*len(self.basis_functions_labels)
118     wavenum_vec[0], basis_functions[0] = self.GetBasisFunction(path = self.
119 folderpath_baselinecorrected + r'\292nm-EGDMA-ID0187-3_Paul_corrected.dat',
120                             thickness = 292.37)
121     wavenum_vec[1], basis_functions[1] = self.GetBasisFunction(path = self.
122 folderpath_baselinecorrected + r'\dep11_pure_MAA_corrected.dat',
123                             thickness = 2020.0)
124     if self.use_HEMA:
125         wavenum_vec[2], basis_functions[2] = self.GetBasisFunction(path = self.
126 folderpath_baselinecorrected + r'\116nm-HEMA_corrected.dat',
127                             thickness = 67.0)
128     h = 0
129     for k in range(len(self.basis_functions_labels)-1):
130         h += (wavenum_vec[k]==wavenum_vec[k+1]).all().astype(int)
131     if h != len(self.basis_functions_labels)-1:
132         print("Error: wavenumber values don't match")
133         exit
134     wavenumber = wavenum_vec[0]
135     return wavenumber, basis_functions
136 def GetBasisFunctionsATR(self):
137     basis_functions = [None]*len(self.basis_functions_labels)
138     wavenum_vec = [None]*len(self.basis_functions_labels)
139     wavenum_vec[0], basis_functions[0] = self.GetBasisFunction(path = self.
140 folderpath_baselinecorrected + '\pEGDMA_292nm_ATR_corrected.dat',
141                             thickness = 292)
142     wavenum_vec[1], basis_functions[1] = self.GetBasisFunction(path = self.
143 folderpath_baselinecorrected + '\pMAA_dep11_ATR_corrected.dat',
144                             thickness = 725)
145     if self.use_HEMA:
146         wavenum_vec[2], basis_functions[2] = self.GetBasisFunction(path = self.
147 folderpath_baselinecorrected + '\116nm-HEMA_corrected.dat',
148                             thickness = 1)
149     h = 0
150     for k in range(len(self.basis_functions_labels)-1):
151         h += (wavenum_vec[k]==wavenum_vec[k+1]).all().astype(int)
152     if h != len(self.basis_functions_labels)-1:
153         print("Error: wavenumber values don't match")
154         exit
155     wavenumber = wavenum_vec[0]
156     return wavenumber, basis_functions
157 def SaveParameterList(self, parameter_list):
158     with open(self.output_path + 'fitting_results.csv', "w") as file:
159         for k in range(len(self.basis_functions_labels)-1):

```

```

        file.write('F({});F({})_error;'.format(self.basis_functions_labels[k],
self.basis_functions_labels[k]))
155     file.write('d / nm;d_error / nm\n')
        for parameters in parameter_list:
157             F_vec, F_error_vec, d_vec, d_error_vec = parameters
                #format_list = list(itertools.chain.from_iterable([list(a) for a in list
(zip(F_vec, F_error_vec))]))
159             for k in range(len(self.basis_functions_labels)-1):
                    file.write('{:f};{:f};'.format(F_vec[k], F_error_vec[k]))
161             file.write('{:f};{:f}\n'.format(np.sum(d_vec), np.sum(d_error_vec)))
def PlotBasisFunctions(self):
163     fig, ax = plt.subplots()
        for k in range(len(self.basis_functions_labels)):
165             ax.plot(self.wavenumber, self.basis_functions[k], label='A_' + self.
basis_functions_labels[k])
                ax.plot(self.wavenumber, np.zeros(len(self.wavenumber)), 'k')
167             ax.invert_xaxis()
                ax.legend()
169             ax.set_xlabel('wavenumber / cm$^{-1}$')
                ax.set_ylabel('absorbance*d_sum$^{-1}$ / $\mu$m$^{-1}$')
171 def PlotMultiFTIRfitsWithFileDialog(self):
        paths = GeneralFunctions.GetFilepathsWithFileDialog(self.
folderpath_baselinecorrected)
173         paths.sort()
            parameter_list = []
175         for path in paths:
                wavenumber, A_data = self.ReadFTIRdata(path)
177                 parameters = self.CalculateSuperposition(path, wavenumber, A_data)
                    self.PlotSuperposition(wavenumber, A_data, parameters, data_name=os.path.
splitext(os.path.split(path)[1])[0])
179                 parameter_list.append(parameters)
                    if self.save_figure_and_data_flag:
181                         self.SaveParameterList(parameter_list)

183 if __name__ == '__main__':
        subprocess.Popen("Rscript --vanilla C:/Users/Martin/Dropbox/Master-Arbeit/R_programs
/baseline_corr.R", shell = True)
185         FTIRfitter1 = FTIRfitter(use_HEMA = True,
                                use_ATR = False,
187                                save_figure_and_data_flag = True,
                                folderpath_baselinecorrected = r'Z:\MartinT\FTIR\
baselinecorrected',
189                                output_path = r'Z:/MartinT/FTIR/baselinecorrected/
eval_dep32/')
        #FTIRfitter1.PlotBasisFunctions()
191         FTIRfitter1.PlotMultiFTIRfitsWithFileDialog()

```

python/FTIR_plotter_superposition_MAA_EGDMA_HEMA.py

10.4 R script for FTIR baselinecorrection

```
1 #library(Matrix)
  library(baseline)
3
4 path_name_all = "Z:/MartinT/FTIR/"
5 filenames_all <- list.files(path = path_name_all , pattern = "\\\\.DPT$")
  for (i in 1:NROW(filenames_all)){
6   filenames_all[i] <- substr(filenames_all[i],1,nchar(filenames_all[i])-4)
7 }
9
10 path_name_already_converted <- "Z:/MartinT/FTIR/baselinecorrected/"
11 filenames_already_converted <- list.files(path = path_name_already_converted , pattern =
  "\\\\.dat$")
  for (i in 1:NROW(filenames_already_converted)){
12   filenames_already_converted[i] <- substr(filenames_already_converted[i],1,nchar(
    filenames_already_converted[i])-14)
13 }
15
16 filenames = setdiff(filenames_all , filenames_already_converted)
17 if (NROW(filenames)>0){
  for (i in 1:NROW(filenames)){
18   filenames[i] <- paste(filenames[i],".DPT",sep="")
19 }
21
  for (i in 1:NROW(filenames) ) {
22   name <- paste0(path_name_all , filenames[i])
23   data <- read.table(name,dec = ".", sep = "\t")
24   wavenumber <- data[,1]
25   index <- wavenumber>=700 & wavenumber <=4000
26   wavenumber <- wavenumber[index]
27   int <- t(data[index,2])
28   #baselineGUI(int , method='irls' , rev.x = FALSE)
30
31   #int_corr <- baseline(int[, , drop=FALSE] , lambda=6, hwi=200, it=20, int=3000,
    method='fillPeaks')
32   #int_corr <- baseline(int[, , drop=FALSE] , lambda=6, hwi=100, it=10, int=2000,
    method='fillPeaks')#Martin
33   int_corr <- baseline(int[, , drop=FALSE] , lambda=6, hwi=40, it=45, int=2000, method=
    'fillPeaks')#Paul test
34   plot(int_corr)
35
36   export <-cbind(wavenumber, t(int_corr@corrected) , t(int_corr@spectra))
37
38   name_export <- paste0(path_name_already_converted , substr(filenames[i],1,nchar(
    filenames[i])-4),"_corrected.dat")
39   write.table(export , file = name_export , append = FALSE, quote = FALSE, sep = " ",
    eol = "\n" , na = "NA" , dec = ".",row.names = FALSE, col.names = FALSE, qmethod = c("
    escape" , "double") , fileEncoding = "")
40 }
41 }
```

R_programs/baseline_corr.R